1

Materials for Thermochemical and Sorption Heat Storage

Kokouvi Edem N'TSOUKPOE
2iE, Ouagadougou, Burkina Faso

1.1. Introduction

It is easy to understand what a material for storage in the form of chemical potential is: we can find examples in our everyday experience. Just take a look at an application that dates back to the Stone Age: the preparation of whitewash using lime obtained from quicklime. What happens when you mix quicklime with water? We can observe that *heat is released*, which becomes all the more intense when a greater quantity of quicklime is mixed with water. The water may start to boil and give off lime, which has a very base pH level and is in fact corrosive. This is why we are often told to pour the lime powder into the water gradually, and not vice versa. After the reaction of quicklime with water is complete, a paste of slaked lime is obtained. What happens next if we dry this paste by bringing it up to a high temperature? The paste *releases water*, and we end up with the same quicklime we started with. It is therefore possible to wet it again and obtain a release of heat. In summary, when you have quicklime in a bag at room temperature, you can say that you have heat at hand, since at any time when you want to obtain heat, you can just mix it with water. It does not matter how long the lime is stored for; the main issue is to protect it from moisture and air. In this way, the drying process, during which you apply heat to allow the slaked lime to release water and thus to *regenerate* the potential for *water absorption* of the lime, can be considered as a process of

Heat and Cold Storage 2,
coordinated by Nolwenn LE PIERRÈS and Lingai LUO.

recharging the lime with heat. This means that lime is a material that allows heat to be stored.

Quicklime is a powder that is essentially made up of calcium oxide (CaO), while slaked lime is made up of calcium hydroxide ($Ca(OH)_2$). The chemical reaction that occurs during the hydration operation is the following:

$$CaO\ [solid] + H_2O\ [liquid] \rightarrow Ca(OH)_2\ [solid] + heat \qquad [1.1]$$

If the amount of water used is not too great – an amount no greater than what is necessary for it to be *hydrated* (1 L of water for every ~3.1 kg of pure quicklime), the slaked lime that is obtained is also in the form of a powder. This result is generally obtained by spraying the quicklime with water. The amount of heat released is $\Delta H = -65\ kJ \cdot mol^{-1}$ of CaO.

Because of its "thirst for water", lime is sometimes spread onto soils that are too humid in order to reduce their water content, and thus facilitate working on them: it is a *hydrophilic* material.

Another hydrophilic material that can be found frequently in our daily lives is silica gel ($SiO_2 \cdot nH_2O$). It is made up of small translucent pellets that can be found in small packets, which are placed in shoe boxes, electronic equipment, or in bottles containing medical tablets. By absorbing the surrounding moisture, these pellets protect the products from damages that might be caused by the presence or introduction of moisture during the transporting or storage of the product. The water attraction capacity or water sorption capacity of the silica gel is due to its large specific surface area; in other words, the area of the real surface relative to its mass. This area is equal to 600–800 $m^2 \cdot g^{-1}$ (Sun and Meunier 2003), meaning that every 10 g of silica gel, the amount contained in a small spoon, has a surface area equivalent to that of a soccer field (which totals roughly 7,000 m^2 for international competitions)! How is this possible? Apart from the size, shape and volume, which have an obvious impact on the *specific surface area*, irregularities or roughness on the surface can greatly influence the actual surface area offered by a particle, and therefore its specific surface area. To demonstrate this, let us consider the beads from the same material, as shown in Figure 1.1. The sizes of the irregularities have been exaggerated for ease of viewing, since at the macroscopic scale, observers perceive them as identical spherical balls (shown with a dotted outline). Thus, the bead presented in Figure 1.1(b) has an irregular contour, which is longer than the

bead shown in Figure 1.1(a), and the bead (b) contains a larger external surface area than the ball (a). This is considered to be external surface roughness. In the case of the bead (c), there are also "internal" surfaces connected to the external surface by "passages" which are known as *πόρος* (*poros*) in Greek, a name which also evokes words such as "portal", in the sense of a passageway, or "to carry", referring to transportation. Because of this, we use the word *pores* to refer to cavities, canals, or ducts that are deeper than they are wide (Rouquerol et al. 1994), according to the definition established by the International Union of Pure and Applied Chemistry (IUPAC). Bead (d) contains a certain number of closed pores, which are totally isolated from the others in such a way that no external flow of fluids can access them, and no external gas adsorption can occur there. These closed pores do not contribute to the specific surface area, which focuses on accessible surfaces (Rouquerol et al. 1994).

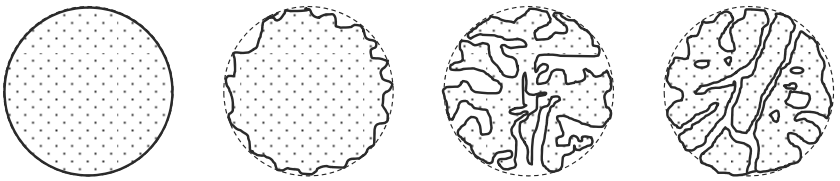

Figure 1.1. *Origin of the specific surface area for a grain of a fixed size of a given material*

One last everyday experience – it depends a lot on where you are! – is the ignition of charcoal. In some large African cities, especially in the West African coastal countries, cooking is primarily done using charcoal as fuel. For ignition, the charcoal is lightly soaked with lamp oil, and it needs to be quickly ignited with a match – or another igniter – otherwise, the flame does not catch and the charcoal quickly seems dry. Indeed, the oil used as lighter fluid is quickly "absorbed" by the coal and disappears in a short time. It is then necessary to soak it again when the fuel is on the outer surface, or not too far down in the pores. This experiment shows that while the charcoal is not specially prepared in such a way as to have a high sorption capacity, it is sufficiently porous and absorbs oil quickly. On the other hand, if any water is accidentally poured onto the coal, the moisture remains apparent (the coal appears wet) and it must then be dried until the coal is fully dry. Coal has a high affinity for lamp oil but not for water.

This chapter is devoted to materials for thermochemical and sorption storage, and begins with the presentation of the key concepts and terminology used in the study of storage materials. It continues with a presentation and a critical analysis of the main criteria for the selection of materials before a presentation on the thermodynamic equilibria of these materials. The next section addresses the materials currently used in the processes developed up to this time, with a particular emphasis on those that are used most frequently. The chapter ends with an introduction to the problem of mass and heat transfers in solid–gas systems and an overview of the material classification techniques for thermochemical and sorption storage.

1.2. Definitions and key concepts

Chemical energy storage uses invertible chemical reactions[1] to store heat. Depending on the form of the energy supplied to the reaction, we will use the terms thermochemical storage (thermal energy), electrochemical storage (electrical energy) or photochemical storage/photosynthesis (electromagnetic radiation) (Figure 1.2).

Sorption is the retention of gas (the sorbate) by a solid or a liquid (the sorbent). It can involve either absorption or adsorption. The latter, a surface phenomenon, is generically defined as the retention of gas or liquid by a solid or a liquid by surface adhesion. More typically, it is the retention of gas at the surface of a solid or a porous material. We use the terms chemical adsorption (chemisorption) when the phenomenon involves covalent bonds, and physical adsorption (physisorption) when it instead involves Van der Waals forces. Absorption refers to a phenomenon in which a substance (a liquid or gas) penetrates into another (a solid or liquid). In heat storage applications, absorption generally corresponds to the absorption of a vapor by a liquid. Chemical sorption involves more energy than physical sorption. It is characterized by a variance equal to 1. Thus, a single state variable (such as temperature or pressure) is all that is needed to describe a chemisorption

1 A reaction is said to be invertible if it can occur in two opposite directions ($A \rightarrow B$ or $B \rightarrow A$) by modifying/reversing the operating conditions, particularly the pressure or the temperature in the cases that interest us here, without going through the same intermediate equilibrium states. This term is used here to avoid confusion with the term “reversible”, which is a notion specific to thermodynamics.

equilibrium, while two are required (such as temperature, pressure, or concentration of the sorbate in the sorbent) to describe a physical sorption equilibrium. Section 1.4 will be devoted to the thermodynamic equilibria that are relevant to thermochemical heat storage materials.

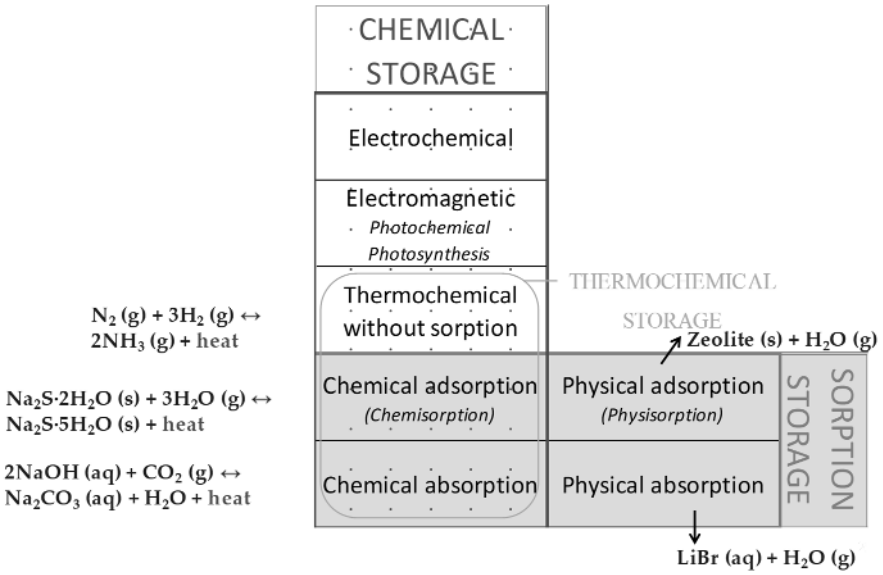

Figure 1.2. *Classification of chemical storage and sorption storage using illustrations: s = solid; aq = aqueous solution; g = gas. Some phenomena, such as storage through photosynthesis, are not reversible*

Several adsorbents are obtained through the agglomeration of microporous crystals to obtain macroporous pellets or granules (Ruthven 1984; Sun and Meunier 1987; Thomas and Crittenden 1998). In this arrangement, the micropores are inside crystals or microparticles, while macropores exist between the crystals, which is to say that they constitute the inter-crystalline space. In the case of the physisorption, depending on whether the physisorbent has one level of porosity (macropores, for example silica gel and active coal) or two levels of porosity (macropores and micropores, for example zeolite), the sorption mechanism is not the same. In the case of a double porosity physisorbent or bidisperse physisorbent, macropores are useful for transporting the sorbate towards the micropores, which provide adsorption capabilities (Sun and Meunier 1987; Silva and

Rodrigues 1999). Figure 1.3 illustrates the general principle of the adsorption mechanism for a physisorbent with double porosity. The adsorbable material, which is to say the potential adsorbate that is not yet adsorbed, diffuses on the surface of the grain with a possible surface resistance. Then it diffuses into the macropores between the particles. The adsorbable reaches the surface of the microparticles and diffuses into the micropores before the intrinsic adsorption on the surface occurs.

For thermochemical reactions such as those involving salt hydrates, which are by far the most commonly used materials in thermochemical energy storage applications for residential applications, an additional phenomenon in in how they are transported must be taken into account. The water is transported through the crystal lattice, forming or breaking bonds. For the dehydration of various salts, a rearrangement of the crystal lattice has been observed, as illustrated in Figure 1.4 for the reaction of the change of $MgCl_2 \cdot 6H_2O$ into $MgCl_2 \cdot 2H_2O$ (Sugimoto et al. 2007). The resulting resistance in the transporting of water vapor is limiting when the crystals are thick.

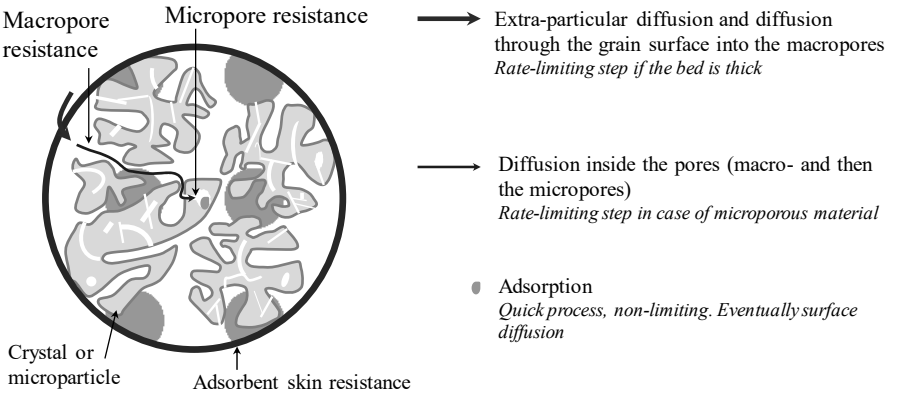

Figure 1.3. *Adsorption in a physisorbent with double porosity. For a color version of this figure, see www.iste.co.uk/lepierres/heat2.zip*

For the sake of simplicity, the expressions “thermochemical storage” and “sorption storage” will be used here interchangeably unless explicitly stated otherwise.

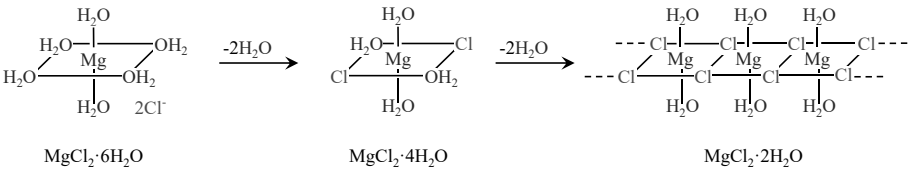

Figure 1.4. *Structural rearrangement during the dehydration of the $MgCl_2 \cdot 6H_2O$ to $MgCl_2 \cdot 2H_2O$ (Sugimoto et al. 2007)*

Therefore, sorption storage or thermochemical heat storage is based on invertible physicochemical phenomena:

$$AB + \text{heat} \leftrightarrow A + B \qquad [1.2]$$

Heat is supplied to the compound AB (a sorption couple or solid–gas reactive pair), which dissociates while absorbing heat to produce two compounds, A and B (equation [1.2] in the forward direction), which can be stored separately: this is an endothermic phenomenon. When these two products are brought into contact, the reverse phenomenon can occur, causing the reformation of the compound AB, releasing heat. During the charging period, heat is supplied to the compound AB in the reactor. Compound B is released in the form of a gas, but in general it is condensed to reduce the storage volume in the case of closed systems. In open systems, compound B is "stored" in the atmosphere, and its volume is not taken into account in the evaluation of the storage density. Since the energy is stored in the form of chemical potential, there are no thermal losses during the storage phase, that is, after the end of the charging and before the start of the discharging; any possible thermal losses are only related to the sensible heat which may have been accumulated in the reactants and are therefore theoretically low, even if the tanks are at room temperature. At the time of the heat demand, the vapor compound B is transferred to the reactor and the compound AB is formed with the release of heat.

In practice, in the thermochemical heat storage processes that have been developed up to now, in almost all cases the sorbate that is used is water because of its many useful qualities, particularly its high availability, its low cost and especially its lack of toxicity, as most of the processes have been developed for "low temperature" applications in households. Thus, the vast majority of research on thermochemical heat storage was focused on

long-term applications for housing. Even in high temperature applications, water is the predominant sorbate, although other fluids are also used. For example, the reaction between quicklime and the sorbate CO_2 is considered for thermochemical heat storage in photovoltaic power plants (Fernández et al. 2019) with desorption temperatures reaching up to 950°C.

1.3. Material selection criteria and review of important characteristics for a thermochemical heat storage material

1.3.1. *Selection and overview of key material properties by application*

Regardless of the energy storage method, the selection of the storage material is seen as an important step in the design of the storage process, because this choice affects both the technical and economic performance of the system. Suitable material must therefore store heat without loss and be able to immediately release it on demand at the desired temperature level, and also not generate any harmful effects. The technical, economic or ecological criteria that generally apply to any type of energy storage are (N'Tsoukpoe et al. 2021):

– the thermal storage density, which indicates the amount of energy stored per unit of volume or mass. Mass is an important data point for applications in terms of material costs. The volume becomes more important in cases such as when the system must be installed in a reserved area or when space is expensive, especially in urban areas. It also has an impact on the cost of the installations, especially when it comes to maintaining excessive operating pressures. The thermal storage density is highly dependent on the operating temperatures;

– high thermal conductivity for a good heat transfer and high specific power;

– environmental safety, non-toxicity, a low global heating potential and a low ozone depletion potential. This component involves aspects concerning the intended use of the material at the end of the system's lifespan and the social impacts of its operation and availability;

– the non-corrosiveness of the materials with respect to those commonly used in the design of system components (tanks, piping, etc.);

– good thermal and chemical stability and good cyclability under operating conditions (temperature, pressure): the material should not lose its

properties, in particular thermophysical/thermochemical properties after successive cycles of charging and discharging;

– a moderate level of the operating pressure range: if possible, avoid excessive pressure conditions, high vacuums or high pressures;

– low costs for the material: this not only applies to obtaining the material, but also to the costs induced over the entire lifecycle of the process. For example, the consumption of pumps or auxiliaries, and therefore the electrical coefficient of performance, depends on the viscosity, the thermal mass capacity and the density when the storage material is a fluid to be circulated, etc.

Depending on the storage method, other specific criteria may also be considered. For the selection of the sorption pair, in addition to the criteria previously stated, other desirable characteristics of sorption pairs include:

– a sorbent with high affinity for the sorbate, which is important in order to obtain a high specific power;

– thermodynamic equilibrium conditions compatible with the operating temperatures targeted by the process: a regeneration temperature (charging) that is as low as possible and a restoration temperature (discharging) that is high enough to satisfy the needs of the intended use. For a closed system (which will be defined in Chapter 3), the specification of these temperatures is equivalent to the definition of the vapor pressures of the sorbate during charging/discharging. On the other hand, in an open system, the relative humidity of the air is generally used, which is equivalent to a partial pressure of water vapor;

– higher sorbate volatility compared to the sorbent in the case of absorption: this eliminates or reduces the need for purification/rectification of the sorbate released by the endothermic phenomenon;

– the melting temperature of the solid in the case of a solid–gas reaction: often, the material quickly loses its reaction capabilities when it undergoes cycles involving melting.

These criteria are often difficult to reconcile and a compromise is usually necessary.

1.3.2. *Important considerations about certain characteristics and selection criteria for thermochemical heat storage materials*

1.3.2.1. *Binding energy*

Usually, the charging temperature T_c is different from the heat release of discharging temperature T_d. In a thermochemical heat storage process, the charging heat Q_c can be divided into three main parts (Hauer 2007b; N'Tsoukpoe et al. 2012): the binding energy Q_{bind} between A and B, the vaporization heat Q_{vap} of the element B and a portion of sensible heat Q_{sen}. The binding energy is lower in the case of physisorption (Van der Waals forces) than in the case of chemical reactions (covalent forces). Typically, it represents between 15% and 30% of the total heat required for the decomposition of salt hydrates, while representing less of it (5%–15%) in the case of physisorption (N'Tsoukpoe 2018; N'Tsoukpoe and Kuznik 2021). In the latter case, the share of the binding energy depends on the change in the concentration defined by the operating temperatures. The heat needed for the vaporization of the element B typically represents between 65% and 85% of the total heat required for the decomposition of salt hydrates (N'Tsoukpoe et al. 2016; N'Tsoukpoe and Kuznik 2021). The sensible heat necessary to raise the temperature of the material in the reactor from its initial temperature (which is usually ambient temperature) to the charging temperature T_c should not be neglected, especially since the process is not continuous. For chemical reactions with salt hydrates, it represents between 3% and 11% of the total heat required for desorption (N'Tsoukpoe 2018). The proportion of this sensible heat is proportional to the temperature difference between the initial temperature of the reactor and the charging temperature. In the case of an absorption process based on the LiBr–H_2O, this value is more significant (40%), not only because of the temperature difference, but particularly due to the low mixing heat or binding heat Q_{bind} that the phenomena of physisorption present.

The conclusion to be reached is that in a thermochemical heat storage process, the heat actually stored in the process typically represents between 15% and 35% of the total heat required for the decomposition for salt hydrates (N'Tsoukpoe et al. 2016; N'Tsoukpoe 2018), and much less (5%–15%) in the case of physisorption for processes described by different authors (Hauer 2002a; Bales et al. 2005; Fischer 2009;

N'Tsoukpoe 2012, 2018; de Boer et al. 2014; Yu et al. 2014). The thermal efficiency of these processes is therefore affected by this.

1.3.2.2. *Volumetric energy storage density*

The volumetric energy storage density is often crucial, especially for domestic applications, and particularly in cases such as when the system must be installed in a reserved area or when space is expensive, as is the case in urban areas. It also has an impact on the cost of installations from the standpoint of civil engineering. The thermal storage density of the material is not a property of the material: it depends on the operating conditions, particularly the temperatures. For example, considering the pair of $CaCl_2 \cdot xH_2O$, it is possible to obtain a volumetric energy storage density of 464 $kWh \cdot m^{-3}$ of salt under vapor pressure of 12 mbar if the desired discharging temperature is 40°C ($CaCl_2 \cdot H_2O + 3H_2O \rightarrow CaCl_2 \cdot 4H_2O + \Delta h_r$). This density is only 171 $kWh \cdot m^{-3}$ of salt if the discharging temperature is about 60°C ($CaCl_2 \cdot H_2O + H_2O \rightarrow CaCl_2 \cdot 2H_2O + \Delta h_r$). Thus, the energy storage density offered by a salt can change significantly. Indeed, the hydrates involved in the reaction (for a chemical reaction) or the water contents (for physisorption involving water) needed to obtain the temperature level for the application are not the same.

The volumetric energy storage density can be simply defined as the amount of energy (in this case, heat) that can be extracted from the system under consideration, divided by the volume of the system. With regard to the material, several volumetric energy storage densities can be distinguished depending on the volume considered:

– *absolute volumetric energy storage density*: the reference volume is the volume of solid grains, that is to say the volume of the solid matter alone or absolute volume (Figure 1.5), excluding all voids between grains or inside the grains;

– *the apparent volumetric energy density* per unit of volume of solid matter, including the volume of the empty spaces contained in the grains (closed pores);

– *the bulk volumetric energy density*: this takes into account the entire volume occupied by the bed of particles considered, including consideration for the pores and the volumes of the empty spaces between the particles.

This is the reference density when determining the volume to be allocated to the material in a reactor, for example. A bed of spherical particles of equal diameter arranged following a cubic arrangement has a theoretical intergranular porosity (the share of the spaces between the grains) of 48%, while a rhomboidal arrangement leads to a theoretical intergranular porosity of 26%. Porosity is necessary for good material permeability, but having excessively high permeability is unnecessary, given that at a constant particle diameter, a high porosity generally means a reduced amount of material per unit volume (N'Tsoukpoe et al. 2014a).

Each of the energy storage densities shown in Figure 1.5 should in principle be given with respect to the material (AB, A, or B), which occupies the largest volume. For absorption storage, such distinctions are irrelevant, as the volumetric energy storage density is reported for volumes of liquids.

The question of volumetric energy storage density goes beyond the material, because the end user of the system is more interested in the broader assembly of the system as a whole. In this case, the area under consideration expands to the level of the process or system. At the process level, consideration for the volume of the condensed fluid (in the cases studied in this chapter, water) is a minimum requirement for closed processes. We refer to this as *reduced volumetric energy density*. We can also consider only the heat that is actually stored in the form of a chemical potential or binding energy; we will therefore talk about *effective or net energy density by volume*.

The participants in Task 42/24 of the International Energy Agency (Solar Heating and Cooling programme: Compact Thermal Energy Storage: Material Development and System Integration) agreed on the fact that in order to ensure the competitiveness of thermochemical heat storage, the volumetric energy storage density it offers must be four to eight times higher than that of water (Wong et al. 2013), or approximately 360 ± 120 kWh·m^{-3}. However, the boundaries of "energy storage density" remain somewhat unclear in the statement, but one can reasonably assume that it refers to a reduced bulk volumetric energy density.

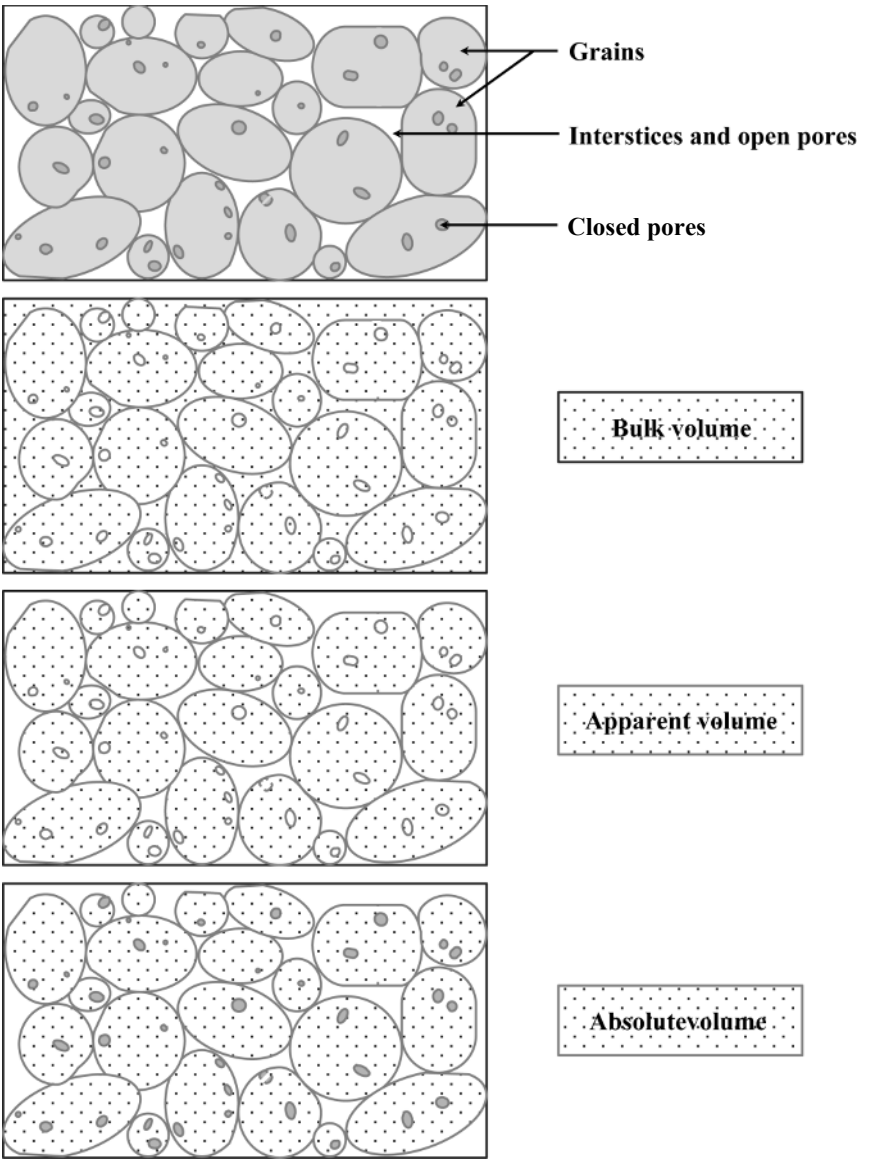

Figure 1.5. *Solid–gas storage: definition of the bulk volume (materials + pores of closed and open pores or gaps between the grains), the apparent volume (grains + closed pores), the true or absolute volume (only the grains outside closed pores) and the volume of the closed pores. For a color version of this figure, see www.iste.co.uk/lepierres/heat2.zip*

1.3.2.3. *The cost of the material*

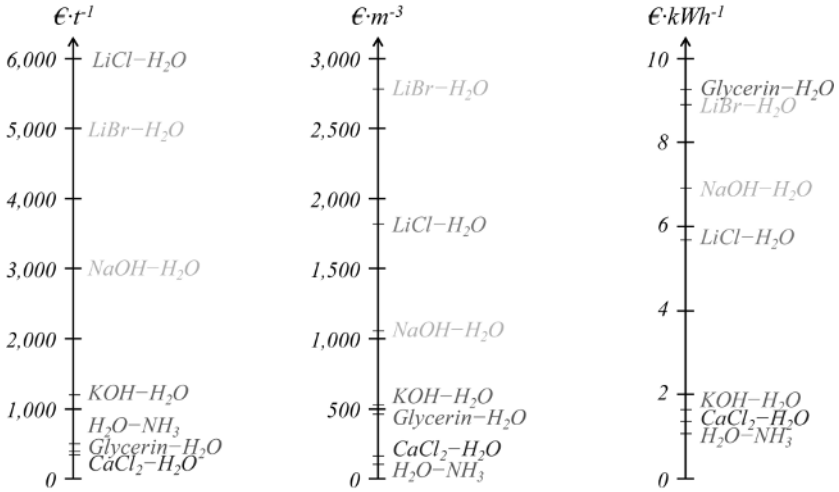

Figure 1.6. *Comparison of the costs for different absorbents in heat storage. For the calculation conditions and price sources, see Table 1.2*

There is currently no definition of a low-cost material. This is mainly due to the fact that the price varies in space and time, as well as the fact that the relevance of the storage will also depend on several local factors, in particular the cost of conventional energy (e.g. the cost of producing heat from fuel oil). To give a clearer idea of this, in the context of Europe at the beginning of the 2010s, the rate of 0.25 €·kWh^{-1} has been deemed as a desirable target rate by various authors (Hauer 2010; Zondag et al. 2010). More recently, within the same context and in various scenarios, this rate was actually 0.60–1.43 €·kWh^{-1}, which was proposed by a group of experts from Task 42 of the International Energy Agency Solar Heating and Cooling Programme (Rathgeber et al. 2015, 2016; Van Helden and Rommel 2015). All such costs are expressed in €·kWh^{-1}, since the common reference to the processes being compared is the amount of stored heat (N'Tsoukpoe et al. 2014b). This makes it possible to take into account the thermal storage density and immediately see the material that will result in a higher investment cost for a given thermal energy storage project. For example, in a study shown in greater detail in section 1.5, the cost of glycerin is 500 €·t^{-1} (Figure 1.6) and allows a storage density of 54 kWh·t^{-1}. Under the same conditions, the LiCl costs 6,000 €·t^{-1} and allows a storage density of 1,053 kWh·t^{-1}. Glycerin is the most expensive material for storage, since for each kWh of heat stored

and assuming a single cycle, it is necessary to invest €9.3, while LiCl requires €5.7. These illustrations show that the selection of the material based on the cost of the purchase or acquisition of the material, in terms of the price per unit of mass (€·kg^{-1}) or per unit of volume (€·m^{-3}), can be misleading. The question of cost should be analyzed over the entire lifecycle of the planned storage, and the important data available should be used for this purpose. A material may very well have a low cost per kWh of stored heat but be highly corrosive and operate under high vacuum, requiring the use of materials resistant to its corrosiveness for the construction of heat exchangers or the reactor, and requiring special components to withstand high vacuum.

1.4. Description of the thermodynamic equilibrium of sorption materials

As indicated previously, the phenomena of chemisorption are monovariant phenomena, while the phenomena of physisorption are divariant. Thus, one state variable (such as temperature or pressure) is all that is needed to describe a chemisorption equilibrium, while two are required (such as temperature, pressure, or concentration of the sorbate in the sorbent) to describe a physical sorption equilibrium. To describe the liquid–vapor or solid–gas equilibria, simplified forms of the Clapeyron equation are used, and the associated diagrams simplify the study of sorption cycles involving these equilibria. In particular, the Clausius–Clapeyron equation (equation [1.3]) is commonly used to describe the liquid–vapor equilibrium or phase change phenomena of a pure substance when far from the triple point, and where the vapor phase can be assumed to be an ideal gas:

$$\frac{\mathrm{d}P_{eq}}{\mathrm{d}T} = \frac{P_{eq} \cdot \Delta H}{R \cdot T^2} \qquad [1.3]$$

where T is the temperature, P_{eq} is the saturated vapor pressure of the pure substance at the temperature T and ΔH is the specific enthalpy of the phase change at the temperature T.

1.4.1. *The case of chemisorption*

If we assume that the specific enthalpy of the phase change is constant, that is, independent of the temperature, an assumption that can be verified by

the small temperature variations that generally occur in sorption thermal storage processes, we may then integrate equation [1.3] to obtain Rankine's formula:

$$\ln\left(\frac{P_{eq}}{P_0}\right) = -\frac{\Delta H_r}{R}\cdot\left(\frac{1}{T_{eq}}-\frac{1}{T_0}\right) = -\frac{\Delta H_{r0}}{RT_{eq}}+\frac{\Delta S_{r0}}{R} \qquad [1.4]$$

Rankine's formula, usually referred to as Clausius–Clapeyron, the formula from which it derives, is generally used to describe the equilibrium conditions of chemisorption phenomena. In equation [1.4], T_{eq} is the equilibrium temperature (of the sorbent, which is to say, solid or liquid), P_{eq} is the equilibrium pressure of the gas (sorbate) above the sorbent, ΔH_{r0} is the enthalpy of the reaction per mole of gas and ΔS_{r0} is the entropy of the reaction per mole of gas. T_0 and P_0 are the temperature and the pressure at the reference point, respectively. ΔH_{r0} and ΔS_{r0} can be determined experimentally, using methods such as thermogravimetric analysis (TGA) in together with differential scanning calorimetry (DSC) (see section 1.7). Alternatively, they can be estimated from the standard enthalpies and entropies of formation of the compounds that can be found in the database of chemical thermodynamic properties of the NBS (currently the NIST) (Wagman et al. 1982). The values ΔH_{r0} and ΔS_{r0} experimentally measured by different authors (Fischer 2009; Dicaire and Tezel 2011; Gaeini et al. 2017) are between 72% and 95% of the value calculated from this database, which is relatively satisfactory for the estimates of the energies involved, in particular for the energy storage density.

The equilibrium points are generally represented in a pressure–temperature diagram, which is known as the *Clausius–Clapeyron plot*. By choosing $-1/T$ for the temperature scale and ln (P) for that of the y-axis, the equilibrium for each reaction is represented by a straight line following equation [1.4], as illustrated in Figure 1.7.

EXAMPLE.– Estimate the equilibrium temperature of the $SrBr_2{\cdot}6H_2O$ under a saturated water vapor pressure at 10°C. First, we identify the curve for the reaction $SrBr_2{\cdot}H_2O + 5H_2O \rightarrow SrBr_2{\cdot}6H_2O + \Delta h_r$, and then the saturation curve for pure water in Figure 1.7. Using this second curve, the saturation vapor pressure of water at 10°C could be found, approximately 12 mbar. From this, the equilibrium temperature corresponding to $SrBr_2{\cdot}6H_2O$ is $T_{eq} = 45$°C.

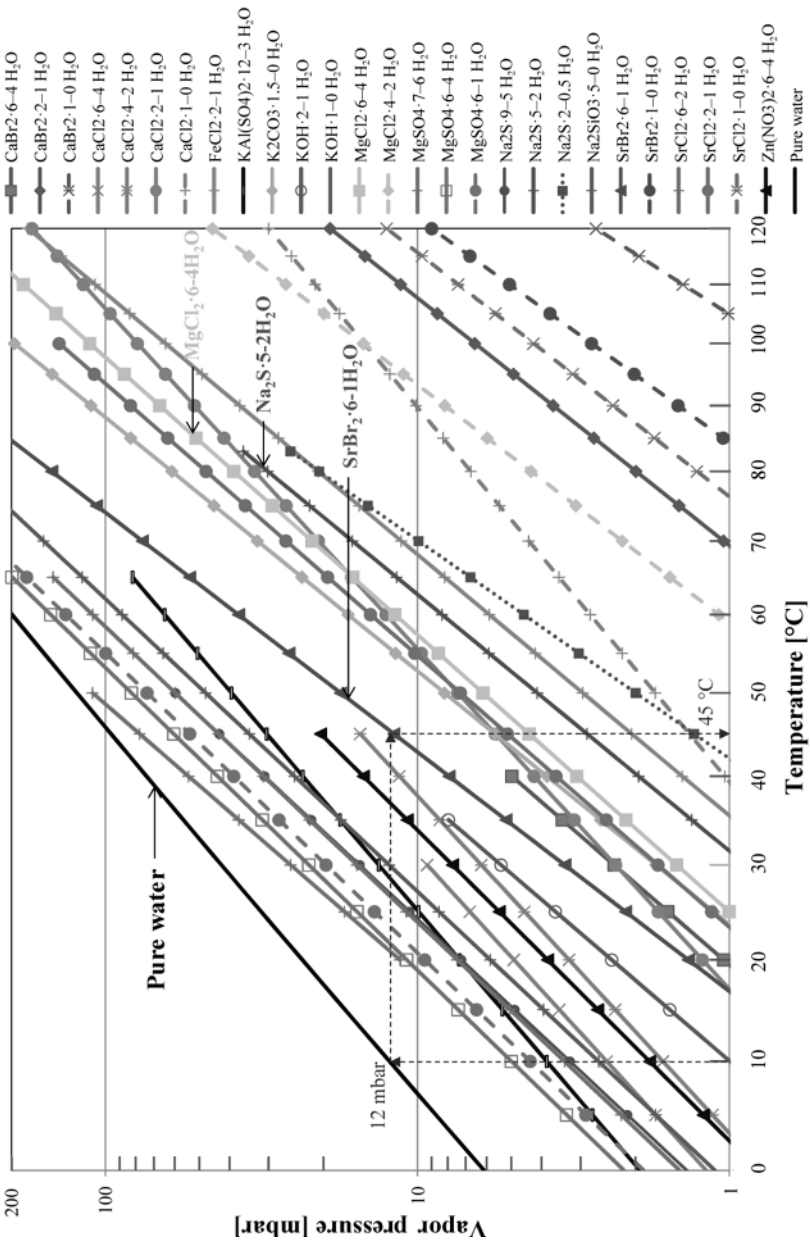

Figure 1.7. *Solid–gas equilibrium curves of salt hydrates in a Clausius–Clapeyron diagram, mostly constructed from the calculated data from the NBS database. For a color version of this figure, see www.iste.co.uk/lepierres/heat2.zip*

1.4.2. *The case of physisorption*

The equilibria of physisorption involve the pressure P, the temperature T and the composition X. This last variable accounts for the amount of sorbate that is sorbed by the sorbent. Since physisorption phenomena are divariant, it is necessary to define two of these three parameters in order to deduce the third; in other words, these equilibria obey laws following the form $P = f(T, X)$.

1.4.2.1. *The case of physical absorption*

In the study of liquid–gas mixtures, the composition is usually taken into account using the mass fraction, which we will also refer to – though some chemical purists will object to this naming! – as concentration or mass content. In a mixture, the mass fraction of a constituent is the mass of this constituent divided by the total mass of all constituents in the mixture, and is denoted as w, according to the recommendation of the IUPAC (International Union of Pure and Applied Chemistry 2014). For example, when we dissolve 30 g of anhydrous lithium bromide (anhydrous LiBr) in 70 g of water, we obtain a solution whose mass fraction in LiBr is $w_{LiBr} = 0.3$. By multiplying this number by 100, we obtain the mass percentage, which is denoted w%, or in this case: $w\%_{LiBr} = 30\%$. Other formulations of properties (such as Patek and Klomfar (2006)) use the molar fraction instead, which is denoted x, that is to say the ratio of the number of moles of the constituent considered relative to the total number of moles. It should be noted that not all authors adopt the same notation, and that it is therefore necessary to carefully check the definitions of the variables used. For example, in this chapter, the molar fraction is denoted X. In the study of absorption processes involving binary mixtures (Chapter 2), the concentration of a solution is usually given relative to the most expensive constituent. Thus, for a LiBr–H_2O mixture (aqueous solution of lithium bromide) where the water is the sorbate, the concentration will instead be given by referring to the mass fraction of the salt (lithium bromide). On the other hand, for the absorption pair H_2O–NH_3 (aqueous ammonia solution) where the ammonia is the sorbate, the concentration will instead be given by referring to the mass fraction of ammonia.

The Clausius–Clapeyron equation also applies to absorption equilibria by treating a mixture of a given concentration as a pure substance. Indeed,

the enthalpy and the entropy of the sorption depend on the concentration of the solution. The representation of these constant composition lines in the (ln(P) *versus* –1/T) plane gives us the *Oldham diagram* of the mixture. In this diagram, the constant composition lines are therefore very close to straight lines, which makes them easier to interpolate. Figure 1.8 shows the Oldham diagram of the NaOH–H_2O pair (an aqueous solution of sodium hydroxide or caustic soda).

Another way of representing the binary mixture equilibria is to use the *Dühring plot*. It translates Dühring's rule, which implies that for a given pressure, the equilibrium temperature of the solution of the binary mixture is a linear function of the saturation temperature of the pure solvent at the same pressure. It follows that in a diagram in which the temperature of the solution is on the *x*-axis and the saturation temperature of the solvent is on the *y*-axis, the constant composition lines are parallel straight lines.

Compared to the Oldham diagram, it has the advantage of using linear coordinates (the temperatures) while maintaining the linearity of the constant composition lines. A secondary axis can be added to give information on the saturation pressure corresponding to the sorbate. It can be observed that Dühring's rule also derives from the Clausius–Clapeyron relation. For the aqueous solution of LiBr–H_2O, for example, the slope of the straight lines is approximately 1.1, which can simplify some thermodynamic analyses of the processes (Anies 2011). Figure 1.9 shows the Dühring's plot of the absorption pair LiBr–H_2O.

1.4.2.2. *The case of physical adsorption*

In the case of physical adsorption, it is also possible to represent the pressure equilibria with an Oldham or Dühring's plot (Figure 1.10). As we have already noticed, this type of visualization facilitates interpolations and is well suited to represent a sorption process, and thus a thermal storage cycle based on sorption.

But here, the concentration is generally the content of the adsorbate, which is to say the amount of adsorbate absorbed per unit of dry mass of adsorbent. For example, when 30 g of water are taken in by 100 g of dry silica gel, the concentration or the water content is X = 0.3 kg of water/kg of silica gel.

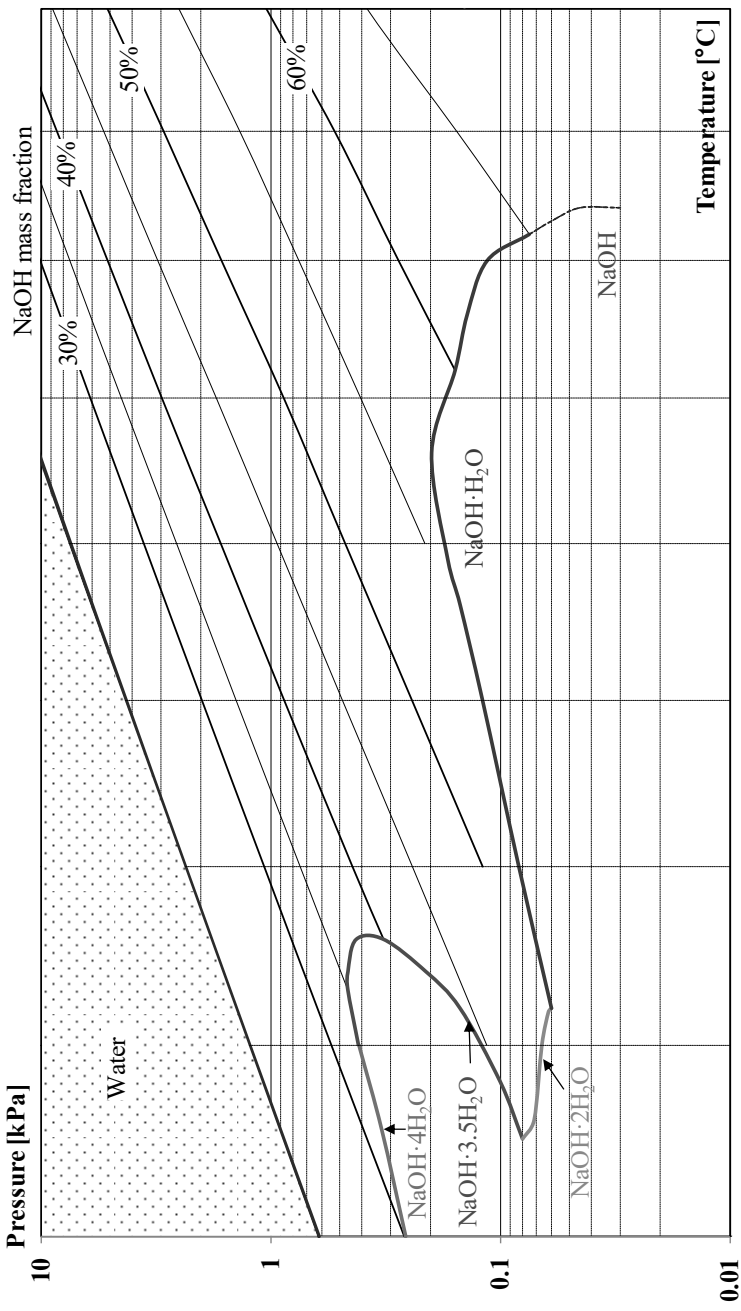

Figure 1.8. *Oldham diagram of the NaOH–H_2O pair. For a color version of this figure, see www.iste.co.uk/lepierres/heat2.zip*

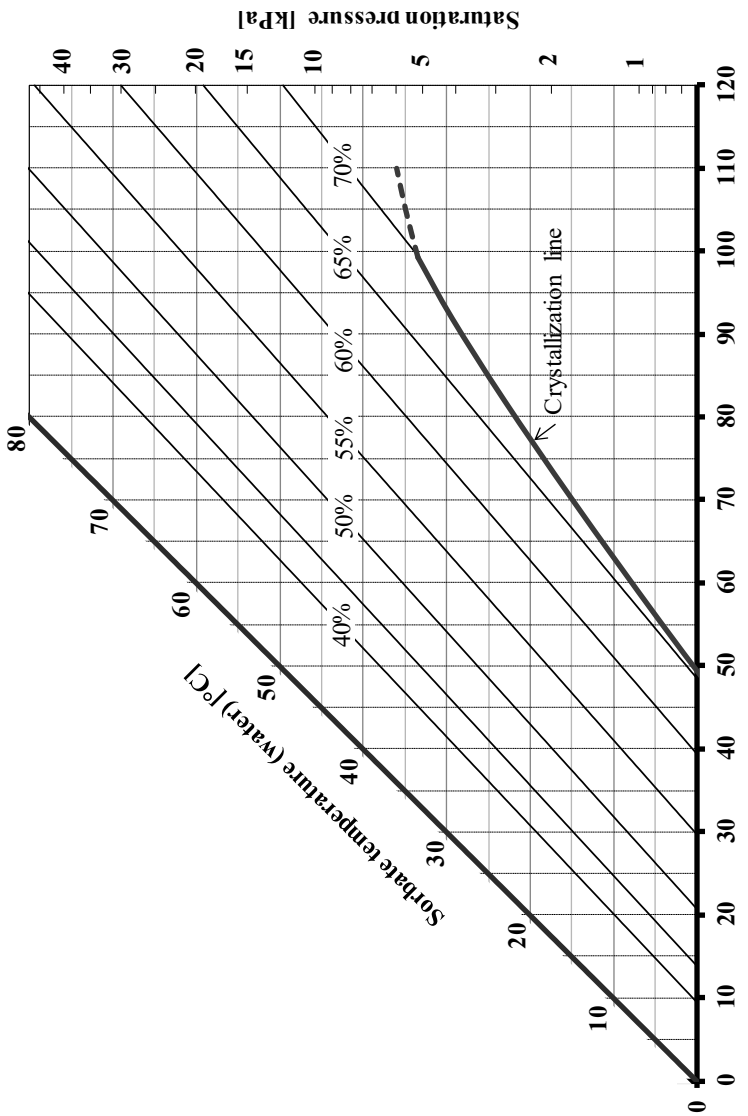

Figure 1.9. *Dühring diagram of the LiBr–H_2O pair*

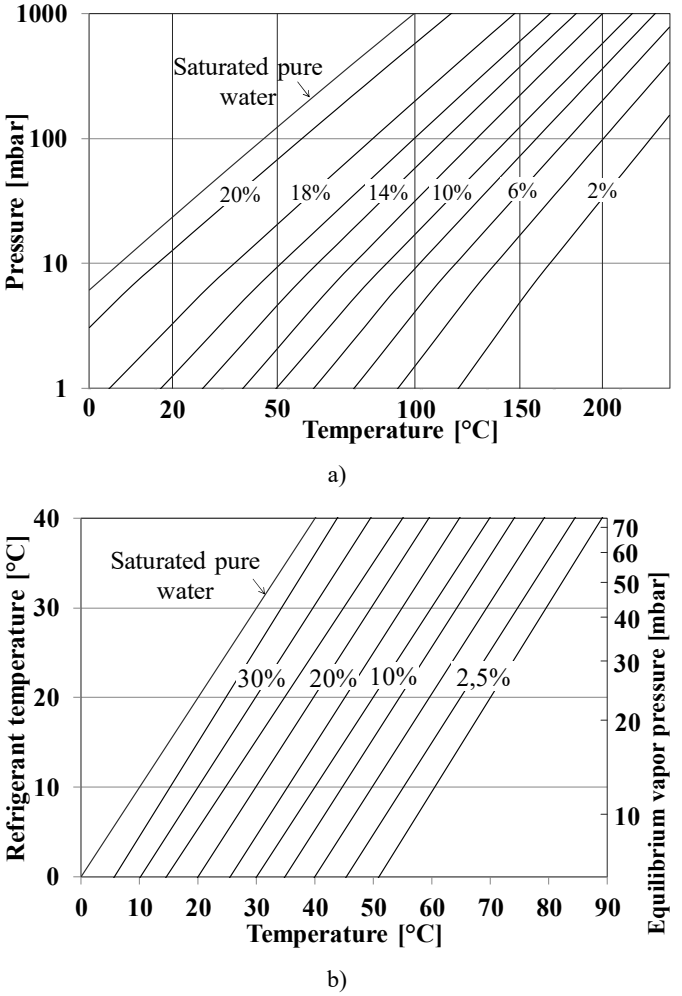

Figure 1.10. *(a) Oldham diagram of zeolite-H_2O pair (Wang et al. 2014) and (b) Dühring's plot of a pair of silica gel-H_2O (Alam et al. 2004)*

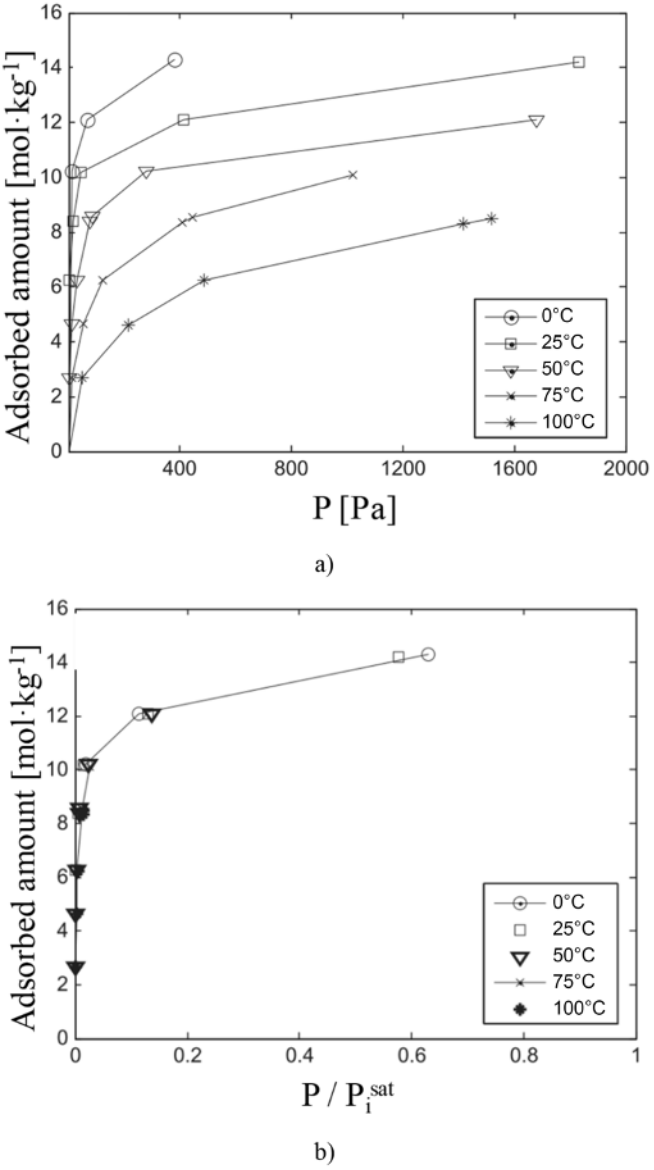

Figure 1.11. *(a) Sorption isotherms of zeolite-H_2O pair; (b) representation of the same points in a diagram introducing the saturation pressure of water (Leppäjärvi et al. 2012)*

Another common way of representing adsorption equilibria, although less convenient for illustrating a sorption cycle or a storage process, is the use of sorption isotherms. Their frequency is linked to the fact that physisorbents are widely used in gas separation processes with adsorption columns operating under isothermal conditions. In this graphical representation, pressure and concentration constitute the axes of the diagram, and the variations at constant temperature – the isotherms, therefore – are plotted (Figure 1.11(a)). There are six main types of adsorption isotherms (Rouquerol et al. 1999), depending on the shape of the isotherm and therefore on the characteristics of the adsorbent. Mathematical models associated with each type of isotherm allow for proposing correlations to represent experimental data as accurately as possible while maintaining physical significance (Sun and Meunier 2003), with model parameters determined experimentally for each adsorption pair. Intermediate isotherms and compound isotherms exist; in fact, this is most often the case, and different types of isotherms can be used to describe parts of an experimental isotherm.

To simplify the models for the simulation, correlations that do not necessarily follow the basic models can be developed. For example, equation [1.5] proposed to describe the sorption equilibrium of the zeolite 13X–H_2O (Tatsidjodoung et al. 2014):

$$X_{eq} = a_2 \cdot T^2 + a_1 \cdot T + a_0 + 0.0228 \cdot \ln\left(\frac{P}{P_{sat}}\right) \qquad [1.5]$$

with X_{eq} being the content of water at equilibrium, T the temperature of the zeolite, P the pressure of the water vapor and P_{sat} the saturation pressure of the water at the temperature T. $a_2 = 3 \times 10^{-6}$ K^{-2}, $a_1 = -0.0017$ K^{-1} and $a_0 = 0.3206$.

In some cases, the data can be reduced to a single curve when the saturation pressure of the pure adsorbate is involved (Leppäjärvi et al. 2012): the unique curve obtained is then independent of temperature. The illustration is shown in Figure 1.11(b) where all the isotherms presented in Figure 1.11(a) are reduced to a single curve. The trick is to switch from the water vapor pressure to the relative pressure defined as the ratio of the water vapor pressure P to the saturation pressure of water at the temperature of the adsorbent, which is equivalent to relative humidity in the case of humid air (Bales et al. 2005).

1.5. Overview of the main materials studied in the context of thermochemical energy storage

Section 1.5 provides an overview of various materials studied in the context of thermochemical heat storage. The goal is not to present an exhaustive list of studied materials but rather to highlight the most representative ones or those that seem to stand out within the considered category.

1.5.1. *Sorbates*

Theoretically, several fluids could be suitable as sorbates in sorption processes (Le Pierrès 2014): water, ammonia, alcohols, alkanes, hydrocarbons, amines, etc. In practice, only water and ammonia are generally used. In a survey of commercially available sorption refrigeration machines compatible with a solar thermal installation, out of around 60 machines, 90% used water as the sorbent, and the remaining 10% operated with ammonia (Mugnier 2013). More specifically, in the context of thermochemical heat storage, water appears to be the fluid of choice; at least for domestic applications, it is the "king" of the sorbates. Its main advantages are obvious.

Table 1.1 presents a comparison with ammonia in the perspective of a thermochemical heat storage application. Ammonia is generally ruled out mainly due to the risks of inhalation poisoning, as even though the odor of this gas is pungent and putrid, making its leak detectable from as low as 5 ppm, intoxication during sleep or an inability to escape is not to be excluded.

Each year, several cases of deaths attributable to inhalation poisoning by gaseous or liquid ammonia are recorded in France, both in professional and domestic environments (Darchy et al. 1997). Apart from chlorine, ammonia is among the gases most frequently involved in accidental domestic poisonings (Tournoud 2008). Although widely used in industry, ammonia is deemed too dangerous for domestic use, and its storage close to places likely to accommodate a large number of people is regulated (Office Fédéral de l'Environnement 2015).

Water	Ammonia
Inexpensive material (++)	Inexpensive materials (+)
Non-flammable (++)	Flammable fluid (–)
Non-toxic (++)	Toxicity to humans and the environment (– –)
Zero potential destruction of ozone layer (++)	Storage subject to regulations (declaration or authorization) (–)
Operation at low pressure, meaning pressures lower than atmospheric pressure in closed systems: limitation of heat and mass transfers, especially in solid–gas reactors, potential sealing problems (–)	Operation at pressure above atmospheric pressure (±)
Suitable thermophysical properties (+)	Suitable thermophysical properties (+)
High heat of vaporization, at about two times that of ammonia (++)	High heat of vaporization, though it is two times lower than that of water (+)
Compatibility with a large number of materials used for civil engineering	Corrosive to copper and copper alloys (–)
Usable for open systems	Impossible to use in the case of open systems

Table 1.1. *Comparison of water and ammonia in the perspective of a thermochemical heat storage application*

Thus, most of the thermochemical heat storage processes are water based. For open processes, as water vapor is naturally present in the atmosphere, this means that once again, water is the preferred fluid. Though water is still the preferred fluid in almost all thermochemical heat storage processes for industrial applications, there are some cases where other fluids are considered. This is the case for CO_2, which has been proposed for thermochemical heat storage in photovoltaic power plants with desorption temperatures of up to 950°C (Fernández et al. 2019).

1.5.2. *Sorption pairs*

1.5.2.1. *Physical absorption*

The absorption pairs considered for sorption heat storage are initially those already used or studied for sorption-based cooling or heating processes (heat pumps). After experiments on these classic sorption pairs, which are relatively few in comparison to the number of studies focused on chemical reactions, there have been some efforts to develop materials specifically tailored for thermal storage by sorption. The first studies on the selection of materials for thermal storage by absorption examined and compared different absorption pairs, such as LiBr–H_2O, NaOH–H_2O, $CaCl_2$–H_2O,

glycerin–H_2O, KOH–H_2O, LiCl–H_2O and H_2O–NH_3 (Liu et al. 2011; N'Tsoukpoe 2012). The main points of comparison between the pairs studied are summarized in Table 1.2. The calculations of the energy storage density are carried out for the same operating conditions (which will be explained in Chapter 2):

– condenser temperature = 30°C;

– minimum heat production temperature in the absorber = 20°C;

– storage tank temperature = evaporator temperature = 10°C.

The detailed approach of the evaluation of the energy storage density is presented by N'Tsoukpoe (2018). The value of 20°C used as the minimum temperature to be provided by absorption is objectively low to meet heating needs. This is explained by the fact that it is the temperature level allowed by considering the $CaCl_2$–H_2O pair. The classical efficiency γ (Table 1.2) is the heat delivered by absorption divided by the heat required for desorption. As previously defined, the reduced volume storage density is the one taking into account the volumes of the tanks containing the solution and water, at their respective maximum capacities during the cycle. The toxicity evaluation is done using the NFPA, which is a standard defining the main risks associated with each product on a scale from 0 (safe) to 4 (very high risks).

An initial comparison is made by considering a crystallization-free storage (Table 1.2). For salt solutions, the maximum concentration in the solution tank is therefore a value close to the solubility limit of the solution at the chosen temperature of the storage tanks, 10°C. For the pairs glycerin–H_2O and H_2O–NH_3, there is no crystallization, regardless of the concentration of the solution. A maximum concentration of 90 w% was decided on, due to the difficulties in reaching a concentration of 100 w%. For the pair H_2O–NH_3, with water as the absorbent, the minimum concentration of NH_3 in the corresponding mixture is therefore 10 w%. The second comparison considers the storage with crystallization in the solution tank, making it possible to increase the energy density storage, which will be discussed in Chapter 2 (section 2.4.1). The prices shown here (Table 1.2) should be considered relative, since they vary over time and space.

Indeed, it is difficult to establish reliable prices for large quantities (several tons to be stored) of products that are not mass-produced. In this case, the price is given for the storage material other than water, considering the same material purity (>99%), on the Chinese market (December 2008).

The LiCl−H_2O and KOH–H_2O pairs have practically the same performance (Table 1.2) in terms of volumetric storage density and efficiency, taking into account the uncertainties on the properties used in the calculations. The disadvantage of the two salts containing lithium is their high cost, likely sustained by the demand for lithium, especially in electrochemical storage applications. The highest viscosity of LiCl raises concerns of lower heat transfer coefficients (Pataskar et al. 2011). The high viscosity also creates a significant load on the solution circulation pumps, which can also be damaged (Pataskar et al. 2011). The mixture of the LiBr and LiCl solutions creates a solution with a higher viscosity than each of them individually but reduces the risk of crystallization for the latter since its solubility range is narrower. Therefore, KOH–H_2O would seem to be the best choice when considering the cost (1.7 €·kWh^{-1}) and the volumetric storage density. Its viscosity is comparable to that of the LiBr solution, but the desorption of this solution requires a higher temperature level.

The LiBr–H_2O pair provides the highest volumetric energy storage density (Figure 1.12) as the heat release temperature increases, with a greater margin for heating (Figure 1.12). For a temperature of 35°C in the absorber, the reduced volumetric storage density is approximately 100 kWh·m^{-3}.

In Figure 1.12, only a few points related to the NaOH–H_2O pair have been represented. Indeed, this solution has a crystallization curve that is in fact very particular (Weber and Dorer 2008; Fumey et al. 2014), and special arrangements are required to practically obtain the point corresponding to 44.5°C (N'Tsoukpoe 2012). The significant issues with severe corrosion and of the particular crystallization curve (Ferchaud 2016) – leading to clogging in pipes and circulators – make this salt less attractive. Figure 1.12 also shows that the storage density becomes zero for a given temperature, generally because the concentrations of diluted and concentrated solutions approach each other, but this is not always the reason. Analyzing closely, for example, the LiBr–H_2O pair, it is observed that beyond this temperature (45.8°C), the "latent" heat (heat of dilution and latent heat provided by the water vapor) is lower than the sensible heat necessary to bring the solution from the temperature of the storage tank to the desired absorption temperature. This implies that the thermal storage by classical absorption based on LiBr–H_2O, or the other pairs of salt solutions presented here, cannot provide heat for DHW applications requiring a temperature of around 60°C (Figure 1.12).

Pair		$CaCl_2$–H_2O	Glycerin–H_2O	KOH–H_2O	LiBr–H_2O	LiCl–H_2O	NaOH–H_2O	H_2O–NH_3
Price (€ per metric ton of storage material)		350	500	1,200	5,000	6,000	3,000	400
NFPA 704	Health	2	1	3	2	2	3	3
	Flammability	0	1	0	0	0	0	1
	Instability/reactivity	1	0	1	0	0	1	0
Storage without crystallization	Concentration after desorption (m%)	39.8	90.0	50.8	58.8	42.8	33.5	90.0
	Desorption temperature (°C)	44.8	53.0	63.0	72.0	63.1	50.0	155.5
	Energy storage density ($kWh \cdot t^{-1}$)	254	54	727	561	1,053	433	366
	Solution energy storage density ($kWh \cdot m^{-3}$)	119	50	313	313	319	154	98
	Reduced energy storage density ($kWh \cdot m^{-3}$)	102	–	217	217	220	126	–

Table 1.2. *Elements of comparison of the various absorption pairs studied*

Pair		$CaCl_2$–H_2O	Glycerin –H_2O	KOH–H_2O	LiBr–H_2O	LiCl–H_2O	NaOH–H_2O	H_2O–NH_3
Storage without crystallization	Cost of storage material (€*kWh^{-1})	1.4	9.3	1.7	8.9	5.7	6.9	1.1
	Pressure during charging (mbar)	42	42	42	42	42	42	1,167
	Pressure during discharging (mbar)	12	12	12	12	12	12	615
	Classic efficiency γ	0.909	0.545	0.830	0.850	0.866	0.750	0.665
Storage with crystallization	Concentration after desorption (m%)	48.5	–	58.8	68.3	51.8	37.8	–
	Desorption temperature (°C)	54.2	–	84.0	91.4	69.4	57.0	–
	Energy storage density (kWh·t^{-1})	562	–	916	725	1,326	662	–
	Solution energy storage density (kWh·m^{-3})	263	–	400	404	401	233	–
	Reduced energy storage density (kWh·m^{-3})	–	–	–	256	255	–	–
	Cost of storage material (€*kWh^{-1})	0.6	–	1.3	6.9	4.5	4.5	–

Table 1.2. *Elements of comparison of the various absorption pairs studied (continued)*

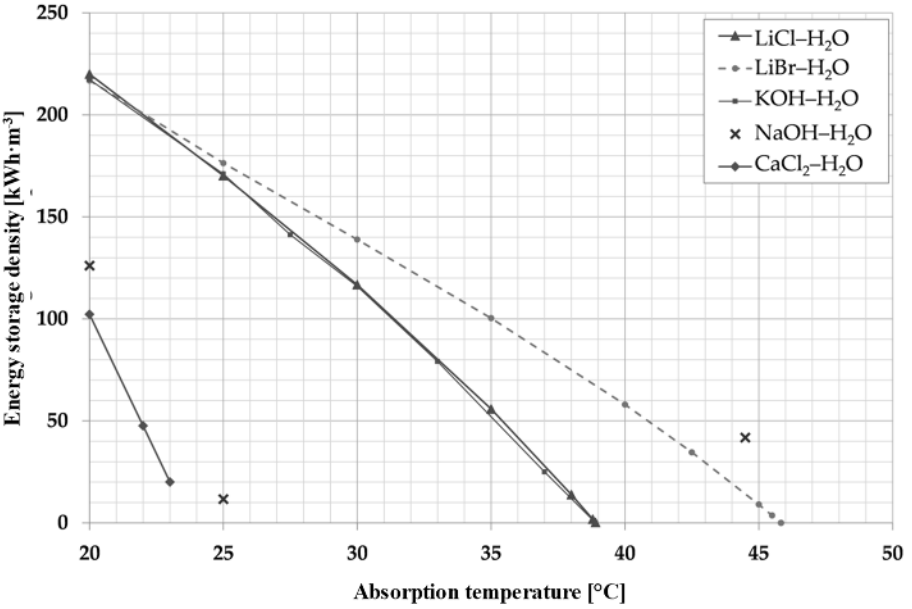

Figure 1.12. *Evolution of the reduced volumetric energy storage density as a function of the absorption temperature for different absorption pairs. Evaporator temperature = storage temperature = 10°C, storage without crystallization (concentration of the solution at the end of charging at the saturation limit). For a color version of this figure, see www.iste.co.uk/lepierres/heat2.zip*

Another limit prevents the use of the aqueous salt solutions currently considered for the production of heat at a temperature level of 60°C, particularly in the case of seasonal storage. This has to do with the saturation curve and the evaporator temperature. Let us consider LiBr–H_2O. If we consider the evaporation pressure corresponding to a temperature of 10°C, the minimum concentration of the solution that would be required would be x = 64.7% at the end of absorption. However, a solution with such a concentration could only be drawn from a storage tank whose temperature is about 40°C (see the Dühring's plot of the pair LiBr–H_2O in Figure 1.10), since this is the saturation concentration of the solution at 40°C. It is difficult to consider maintaining the solution reservoir above such a temperature in ordinary storage, unless the storage of sensible heat is managed with the appropriate insulation. These conclusions also apply in the case of storage using crystallization, which will be discussed in Chapter 2 (section 2.4.1), because the solutions used in the evaluations are already at the saturation

point. One way to overcome this limitation could be the use of additives or mixtures that shift the crystallization curve or inhibit crystallization (Adegoke 1993; Lee et al. 2000; Dirksen et al. 2001; Ring et al. 2001; Chan et al. 2013), which could also allow them to increase the energy storage density.

However, the cost of LiBr is high. In addition, the solution that is formed is viscous and corrosive. The conventional method of thermal storage by absorption therefore offers a thermal storage density comparable to that of sensible water storage when the temperature of the intended application exceeds 40°C. New approaches, both at the material and process/system levels, are essential to make this thermal storage process relevant.

To this end, studies have been undertaken to identify or develop inexpensive sorption pairs capable of offering a higher energy storage density (Lefebvre 2015) for a process involving crystallization. From an initial list of 220 salts, a preliminary selection was made based on arbitrary but reasonable values for different criteria initially defined (Figure 1.13).

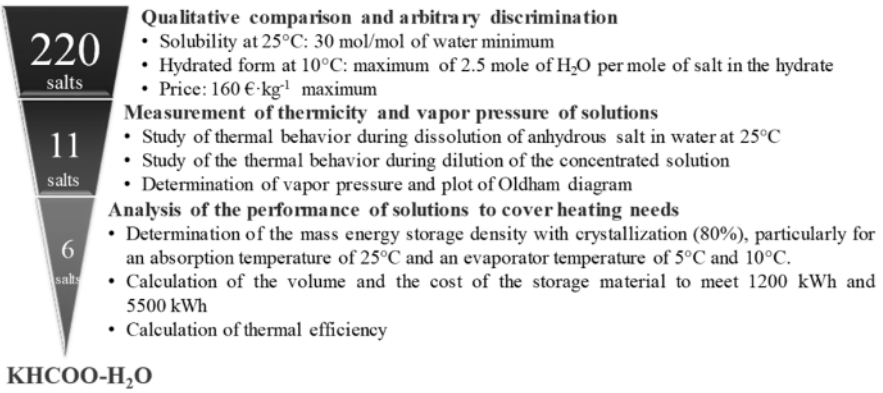

Figure 1.13. *Flowchart of the salt selection process for long-term thermal storage by absorption adopted by Lefebvre (2015)*

These criteria include (i) a minimal solubility of the salt in water to increase the maximum concentration of the solution in the tank, and ultimately the energy storage density, and which is also an indicator of a strong interaction between the water molecules and the salt; (ii) a limited hydration degree, that is to say a low number of moles of water per mole of

salt at the crystallization temperature, again to increase the maximum concentration of the solution in the tank; and (iii) a reasonable price for the anhydrous salt. This step results in a list of 11 "promising" salts, which are LiBr, LiCl, $ZnBr_2$, $ZnCl_2$, KHCOO, KCH_3COO, KSCN, NaSCN, NH_4HCOO, NH_4CH_3COO and NH_4SCN. A second step consists of studying the thermicity of the phenomena involved and the vapor pressures of the salt solutions. It shows that the dissolutions of the various salts in water as well as the dilutions of these salts are exothermic, except for NH_4HCOO, NH_4CH_3COO and NH_4SCN, where at least one of these phenomena is endothermic. The measurement of the vapor pressure of the solutions at different concentrations indicates a high vapor pressure value for KSCN and NaSCN, which makes them not very favourable for thermal storage by absorption. Finally, six salts underwent a more in-depth analysis, including the determination of the quantity of salt required to store 5,500 kWh and 1,200 kWh. The material costs, as well as the associated storage volumes, are also determined.

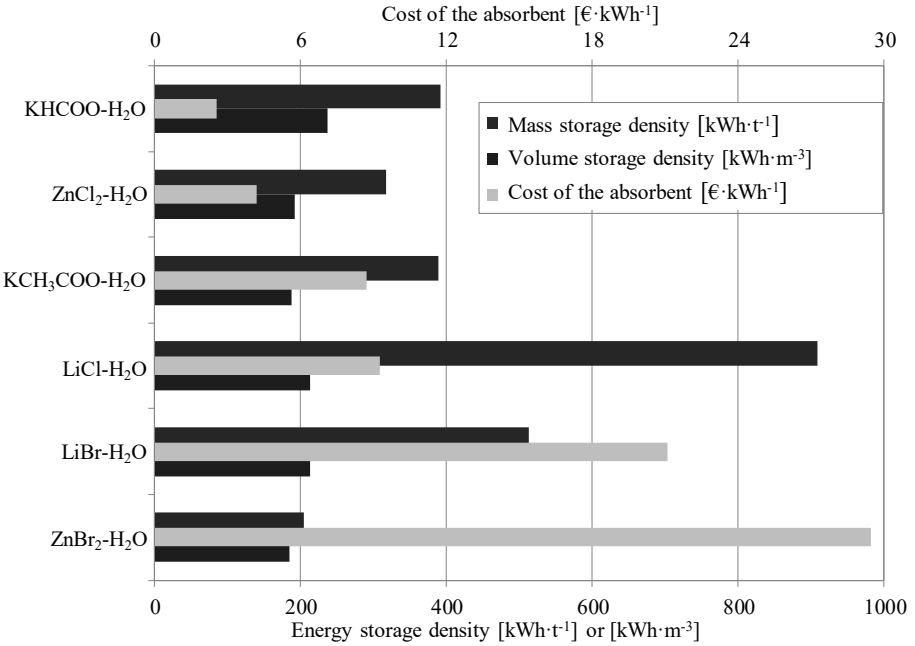

Figure 1.14. *Comparison elements of the main pairs with potential for thermal storage by absorption in the study by Lefebvre (2015). For a color version of this figure, see www.iste.co.uk/lepierres/heat2.zip*

It appears that LiBr and LiCl offer the best volume or mass energy storage densities, but are very expensive (Figure 1.14), meaning that it is unlikely that they could be considered for any commercial applications. It should be noted that, unlike the previous analysis, whose results are presented in Table 1.2, the current analysis assumes that the purchase price of LiBr (10,600 €·t^{-1}) is higher than that of the LiCl (8,400 €·t^{-1}). Conversely, $ZnBr_2$ and $ZnCl_2$ have a low volumetric energy density, requiring at least 9.4 m^3 of storage volume (water + solution) to store the 1,200 kWh to be released at 25°C under an evaporator at 10°C; their total cost is also high. Finally, it is KHCOO which offers a cost advantage and was therefore selected, despite its comparatively low thermal storage density (Figure 1.14).

1.5.2.2. *Physical adsorption*

According to the classification of the IUPAC (International Union of Pure and Applied Chemistry 2014), adsorbents can be microporous (pore size < 2 nm), mesoporous (pore size: 2–50 nm), or macroporous (pore size > 50 nm). Currently, silica gel and zeolite are the two main physical adsorbents considered for thermal storage processes by physical adsorption. This is already the case for adsorption-based cooling processes, where a study (Mugnier 2013) listing commercial machines indicates that out of the 12 machines surveyed, three operated with silica gel–H_2O, and the other nine used zeolite–H_2O. The main difference between zeolite and silica gel is that zeolite consists of microcrystals and, therefore, has a uniform pore size, while silica gel is an amorphous material with a pore size distribution ranging from micropores to macropores (Table 1.3). There are also aluminophosphates (Table 1.4), which are examined to a lesser extent for heat storage, as well as other adsorbents, including activated carbon, more commonly studied for use as a porous matrix for salts in thermochemical heat storage.

1.5.2.2.1. Silica gel

Silica gel is an amorphous material (Table 1.3), consisting of 99% silica (SiO_2) and hydroxyl groupings (OH), which makes it polar and gives it a greater affinity for polar sorbates, such as water and alcohols. The most widely used silica gels in sorption processes, including in sorption heat storage processes, are type A (from Fuji Davison) and type RD (regular diameter).

Properties	Zeolites	Silica gel
Chemical composition	$M^{+}_{x/n}$ $[(AlO_2^{-})_x(IfO_2)_y]\cdot zH_2O$ where M can be cations like Na^{+}, K^{+}, CA^{2+}, Li^{+}	SiO_2 Chemically inert, no metals or cations present
Chemical stability	Chemically stable in a basic medium, neutral, or slightly acidic	Chemically stable in a basic, neutral, or slightly acidic environment
Mechanical stability	The presence of liquid water can have an undesirable effect on mechanical stability	Gels with narrow pores are unstable when used with liquid water
Pore size	Pores with fixed or homogeneous sizes (crystalline structure) Zeolite A: ~3 Å or ~4 Å or ~5 Å Zeolite X: ~8 Å	Pore size distribution (amorphous structure) between 5 Å and 300 Å Average pore size of the gel with narrow pores: 20 Å Average pore size of the gel with large pores: 110 Å

Table 1.3. *Comparison of zeolites and silica gels (W.R. Grace & Co.-Conn 2010)*

Properties	Zeolites	Silica gel
Specific surface area ($m^2 \cdot g^{-1}$)	800	800 (narrow pore gels) 400 (wide pore gels)
Effective pores ($cm^3 \cdot g^{-1}$)	0.25–0.3	0.4 (narrow pore gels) 1.2 (wide pore gels)
Thermal conductivity ($W \cdot m^{-1} \cdot K^{-1}$)	0.12 (balls)	0.14–0.2
Heat of adsorption for water ($kJ \cdot kg^{-1}$ of water)	4,187	2,512
Specific heat capacity ($kJ \cdot kg^{-1} \cdot K^{-1}$)	0.96	0.92

Table 1.3. *Comparison of zeolites and silica gels (W.R. Grace & Co.-Conn 2010) (continued)*

The thermophysical properties of these two materials are similar, but the RD type has a larger specific surface area and higher thermal conductivity, which is enough to create a significant difference in their adsorption capacity (Wang et al. 2004). Adokou (2020) provides an inventory of properties, particularly adsorption properties, for these two materials, as well as for many other silica gels, including types 3A, A++, A5BW, RD 2060, RD 2560, grade 40 and 127B.

Basically, silica gel is inert and non-toxic. It only poses a health risk when it is saturated with a humidity indicator, such as cobalt chloride, which is a cancer-causing chemical compound (Rao et al. 2006).

Composites	Inorganic nanoporous materials	Polymers
Silica gel Mesoporous silicates Materials made from natural rocks Carbonaceous materials	Zeolites (aluminosilicates) Aluminophosphates Aerogels	Porous organometallic materials (MOF) Polyelectrolytes

Table 1.4. *Classification of physical adsorbents (Zheng et al. 2014)*

1.5.2.2.2. Zeolite

Zeolites (or zeolite) are aluminosilicates which have the general formula $M^{+}_{x/n}[(AlO_2^{-})_x(SiO_2)_y]\cdot zH_2O$ (or $M_{x/n}[(AlO_2)_x(SiO_2)_y]\cdot zH_2O$), where M^{+} represents the compensating cation and n represents its valence.

Zeolite has a crystalline structure with a determined or uniform pore size, unlike silica gel, which is amorphous with a pore size distribution. To achieve zeolites of a suitable size for applications, typically in the millimetre range, small-sized zeolite microparticles are agglomerated with binders to ensure good porosity and sufficient mechanical strength (Figure 1.15(a)). This results in a material with various shapes (Figure 1.15(b)) and dual porosity: micropores within the crystals and macropores between the crystals, meaning in the binder.

Zeolites can be natural or synthetic; there are currently about 48 natural zeolites and nearly 200 synthetic zeolites. However, few of them have been of interest for thermal storage applications; the ones that are of interest are types A and X zeolites. The main difference between types A and X zeolites

is the pore size (Tables 1.5 and 1.6). Each zeolite crystal structure is represented by three letters, such as FAU, LTA, MFI, MEL, FER, LTL, SOO, etc., using the guidelines set out by the Structure Commission of the International Zeolite Association (IZA) (Baerlocher et al. 2007). This nomenclature is based on the ratio between the number of silica atoms and the number of aluminum atoms (Si/Al or y/x ratio) that they contain and on the number of rings formed by the pores.

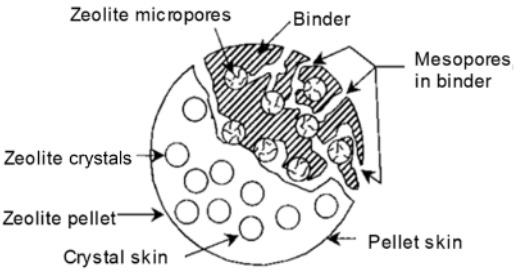

a)

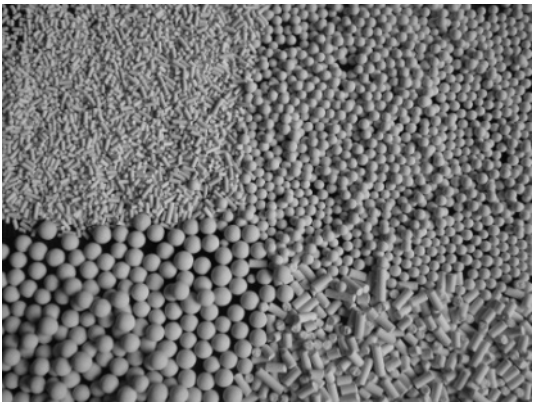

b)

Figure 1.15. *(a) Structure of a zeolite grain (Sircar and Myers 2003); (b) zeolite grains in various forms (photos: courtesy of Pingxiang XINTAO Chemical Packing Co., Ltd.)*

For example, a type A zeolite, which does not have a natural counterpart (Dyer 2001), has a Si/Al ratio between 1 and 1.5 and forms rings with eight oxygen ions. The 3 Å diameter type A zeolite is called zeolite 3A

(Table 1.6). The one with a 5 Å diameter is called zeolite 5A. The MSX (medium silica X) zeolite has a crystalline structure corresponding to the natural faujasite (FAU) zeolite structure, with a Si/Al ratio between 1.05 and 1.15 (Nicolas et al. 2015). Zeolite 13X is also called NaX, with the Na+ cation being predominant in its structure (Table 1.6). Readers interested in nomenclature can refer to general works such as Payra and Dutta (2003).

	Type A	Type X
Chemical composition	$Na_{12}[(AlO_2)_{12}(SiO_2)_{12}]\cdot 27H_2O$	$Na_{86}[(AlO_2)_{86}(SiO_2)_{106}]\cdot 264H_2O$
Pore diameter (nm)	0.3–0.4	0.75 (NaX) 0.10 (CaX)
Specific internal surface area ($m^2\cdot g^{-1}$)	800–1,000	800–1,000
Specific heat capacity ($kJ\cdot kg^{-1}\cdot K^{-1}$)	0.8–0.9	0.8–0.9
Thermal conductivity ($W\cdot m^{-1}\cdot K^{-1}$)	0.58	0.58
Bud bed density ($kg\cdot m^{-3}$)	750	700

Table 1.5. *Characteristics of the different type A and X zeolites*

Zeolite family	Structure of the corresponding natural zeolite	Si/Al ratio	Type of zeolites (examples)	Compensator cation	Pore diameter (Å)
Type A	Sodalite	1	Type 3A	K^+	3
			Type 4A	Na^+	4
Type X	Faujasite	1–1.5	Type 13X	NA^+ majority	~8
		1–1.5	Type 10X	Ca^{2+} majority	10
Type Y	Faujasite	1.5–3	Type Y	Na^+, K^+, Ca^{2+}	7
		>3	Type USY (Ultra Stable Y)	Na^+, K^+, Ca^{2+}	14

Table 1.6. *Classification of type A, X and Y zeolites (Dyer 2001; Sircar and Myers 2003; Hongois 2011)*

1.5.2.2.3. Other physical adsorbents

As previously presented (Table 1.4), there are other physical adsorbents considered for thermal energy storage applications by sorption. However, it should be noted that few authors have focused on them so far. This includes

aluminophosphates, obtained by substituting phosphorus for silicon in the synthesis of zeolites, which are aluminosilicates.

The main advantage of aluminophosphates over their "cousins", the zeolites, is that they offer lower charging temperatures than zeolites, thanks in particular to the S-shape of their isotherms, which characterize type V adsorbents (Aristov 2007; Zheng et al. 2014). They also offer a higher energy storage density than zeolites. However, they are more expensive.

In this family, there are microporous aluminophosphates (AlPO), silicoaluminophosphates (SAPO) and metallic aluminophosphates (MeAPO), such as ferroaluminophosphates (FAPO). Various nomenclatures exist, including those of Union Carbide and IZA, leading to different designations for the same material, and each author or institute sometimes associates its name (MCM-n at Mobil, VPI-n at Virginia Polytechnic Institute, etc.) (Hafida 2008). For example, FAM-Z01 (Functional Adsorbent Material Zeolite 01) refers to FAPO-5, while FAM-Z02 refers to SAPO-34, and FAM-Z05 refers to FAPO-34. Readers interested in this nomenclature can refer to a bibliographic synthesis proposed by Hafida (2008).

There are also polymers (Table 1.4), including porous metal-organic frameworks (MOF) and polyelectrolytes. They have an adsorption capacity of over 80% of their weight with flexibility allowing the attainment of desired sorption isotherms (Zheng et al. 2014). MOFs are composed of different metal ions and organic ligands to form structures in one, two or three dimensions (Batten et al. 2013). They have an excellent water adsorption capacity but exhibit significant hydrophobic lengths at low pressures (Teo et al. 2017). Analyses have shown that MOFs degrade after several dozen cycles (Zheng et al. 2014).

1.5.2.2.4. Use of physical adsorbents in sorption heat storage processes

In the early 2000s, several researchers conducted studies on long-term heat storage using physisorbents (Table 1.7), which are deemed to be more stable than materials involving chemical reactions. Emphasis was placed on silica gels and zeolites, with some large-scale demonstration projects. However, these adsorbent materials proved to be inefficient due to low achieved energy storage densities (Table 1.7), low observed discharging temperatures, especially with silica gel, and charging constraints requiring a high source temperature, especially with zeolites.

Pair	Background and conditions of the study	Performances observed	References
Silica gel-H_2O	Closed system Experimental study of the material and theoretical analyses	Silica gels do not offer any potential for SSCS that would be of interest	(Bales 2008; Gantenbein 2008; Gantenbein et al. 2022)
Silica gel-H_2O	20.4 m^2 of flat plate collectors with DHW Charging: 88°C; Discharging: 42°C Prototypes of HYDES, then MODESTORE	HYDES prototype: 125 $kWh \cdot m^{-3}$ MODESTORE material: 50 $kWh \cdot m^{-3}$	(Gartler et al. 2004; Jähnig et al. 2006; Hadorn et al. 2007; Hauer 2007a; Bales et al. 2008)
Zeolite 13X–H_2O	Charging: 130°C; Discharging: 65°C Storage system for a district heating network	Heating: 124 $kWh \cdot m^{-3}$ Cooling: 100 $kWh \cdot m^{-3}$	(Hauer 2002b, 2007a)
	Charging: 180°C; Discharging: 55°C Closed system Prototype	Material: 180 $kWh \cdot m^{-3}$	(Bales et al. 2008)
	Charging: 180°C; discharging: 20°C	Material: 163 $kWh \cdot m^{-3}$	(Weber et al. 2016; Krese et al. 2018)
	Charging: 180°C; discharging: 57°C	Material: 180 $kWh \cdot m^{-3}$	(Stutz et al. 2017)
Zeolite 13XBF–H_2O	Charging: 190°C; discharging: 28°C T_{ev}: 10°C	Material: 198 $kWh \cdot m^{-3}$	(Gaeini et al. 2017)

Table 1.7. *Data from various sorption heat storage studies on physical adsorbents*

Pair	Background and conditions of the study	Performances observed	References
Zeolite 13X + activated alumina–H_2O	Charging: 250°C Tests with 55g of the AA13X material	Material: 200 kWh·m^{-3}	(Dicaire and Tezel 2009, 2011)
Zeolite MSX–H_2O	Charging: 230°C; discharging: 50–60°C 50 kg of material in an open reactor	Material: 154 kWh·m^{-3}	(Zettl et al. 2014)
Zeolite 4A–H_2O	Charging: 180°C; discharging: ≈ 35°C MONOSORP prototype	120 kWh·m^{-3}	(Bales 2005; Kerskes 2006; Hadorn et al. 2007; Bales 2008)
Zeolite 4A–H_2O	Charging: 230°C; Discharging: 50–60°C 53 kg of material in an open reactor	Material: 148 kWh·m^{-3}	(Zettl et al. 2014)
Zeolite 5A–H_2O	Charging: 103°C; Discharging: 51°C Closed system	Material: 47 kWh·m^{-3}	(Scapino et al. 2017)
	Charging: 180°C; Discharging: 29°C	Material: 83 kWh·m^{-3}	(Krese et al. 2018)
APO-n–H_2O	Charging: 95–140°C; Discharging: 40°C	Material: 240 kWh·m^{-3}	–

Table 1.7. *Data from various sorption heat storage studies on physical adsorbents (continued)*

After some studies on physical adsorbents, including zeolites and silica gel, for thermal storage, the low performances led most researchers to consider the use of these materials only as a support or matrix for other materials with higher thermal storage density, especially salt hydrates, as discussed in section 1.5.2.4.

However, these adsorbent materials have proven to perform poorly because of the low storage energy densities that have been achieved (Table 1.7), the low discharging temperature levels observed (in particular with silica gel) and the charging constraints requiring a high source temperature, particularly with zeolites. After several studies of physical adsorbents for thermal storage, particularly zeolites and silica gel, these outcomes have led most researchers to consider the use of these materials as merely a support or supplement to other materials with a higher thermal storage density, particularly salt hydrates, as discussed in section 1.5.2.4.

At this point, it is worth making note of a reflection made by Aristov (2007) on choosing an adsorbent for energy applications. It is just as fast to select as it is to conceive of the material or materials that may be suitable for a given application based on the shape of the isotherm and the temperature conditions at the limits of the process taken from analytical relationships. According to this analysis, the materials whose sorption isotherms are S-shaped (type V and especially type VI, according to the IUPAC classification) are the materials that are best suited for thermal storage, a consideration which would make zeolites (type I) unattractive (Aristov 2007).

1.5.2.3. *Chemisorption*

The salt hydrates constitute the main class of materials used in heat storage by chemisorption, at least for low-temperature applications, meaning heat levels up to 100–200°C. Beyond 200°C, it is primarily oxide/hydroxide pairs that are employed.

1.5.2.3.1. Hydrated salts for thermochemical heat storage at low temperature

The analysis of the reaction enthalpies of salt hydrates shows that the release of one mole of water is accompanied by an absorption of approximately 55 kJ of heat when there is no particular modification of the salt structure, a value that can reach 74 kJ in certain cases (N'Tsoukpoe et al. 2014b). It follows that salt hydrates capable of releasing a large number of

moles of water under operating conditions potentially offer a significant molar energy storage density. Since the volumetric energy storage density is related to the molar energy storage density, it follows that a salt releasing a large number of moles of water potentially provides a high volumetric energy storage density.

One of the first systematic studies on the selection of salt hydrates for low-temperature thermochemical heat storage was conducted by N'Tsoukpoe et al. (2014b). It is a study of the potential of the family of salt hydrates, taking into account the requirements of the operating conditions of the envisaged system. The approach is based on a three-step process, the essential elements of which are presented in Figure 1.16. This systematic approach has been taken up by other authors, adapted, or further developed for the selection of salt hydrates for thermochemical heat storage (Donkers et al. 2017) or the valorization of the thermal potential of industrial waste heat (Richter et al. 2018).

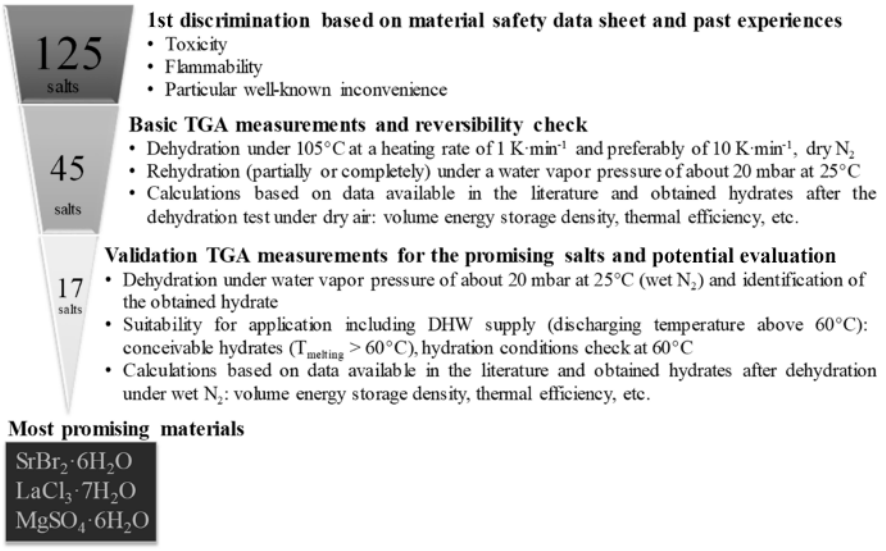

Figure 1.16. *Three-step approach for assessing the potential of thermochemical heat storage materials*

A list of 125 salt hydrates, which can be found in N'Tsoukpoe et al. (2014b), was established from chemistry databases. Initially, materials were eliminated based on general criteria, such as toxicity or flammability, the

risk of explosion, or any particular danger or known problem based on past experiences. Materials exhibiting oxidizing behaviour were also rejected due to issues of cyclability, problems with the reversibility of the reaction after a certain number of cycles having been observed for these materials in previous tests. Only 45 materials (Table 1.8) passed through the filter of this first discrimination step and were thus retained for basic thermogravimetric analyses under dry nitrogen (Figure 1.16). The second and third steps combine theoretical calculations and experimental measurements based on TGA coupled with DSC.

In the second step, the authors conducted TGA/DSC analyses and checked for reversibility of the reactions. The purpose of these basic measurements is to verify the dehydration of the material in the temperature range below 105°C and the possible reversibility of the corresponding reaction with TGA/DSC. Among the 45 salts, 17 showed partial or complete rehydration under a vapor pressure of about 20 mbar at 25°C (Table 1.8). Using data available in the literature, the performance of these 17 salts was evaluated considering the hydrates formed during TGA. Figure 1.17 presents a synthesis of some results obtained, including volumetric energy densities and thermal efficiencies, as defined in section 1.3.2.2. The theoretical effective thermal efficiency η is calculated here by neglecting sensible heats; therefore, it reduces to the reaction enthalpy reduced by the heat of evaporation divided by the reaction enthalpy: this is the part of heat actually stored in the system as chemical potential (bond energy). It immediately appears that the theoretical effective thermal efficiency η of a conventional thermochemical heat storage unit based on salt hydrates below a maximum dehydration temperature of 105°C is relatively low (between 20% and 40%), considering only the heat effectively stored in the system as chemical potential. Two bromides offer the highest efficiencies: 39% for $MgBr_2 \cdot 6H_2O$ and 34% for $SrBr_2 \cdot 6H_2O$. In general, halogenated elements show the best performances (Figure 1.17). There are only three salts ($Zn(NO_3)_2 \cdot 6H_2O$, $CaBr_2 \cdot 6H_2O$ and $SrBr_2 \cdot 6H_2O$) that could provide an effective volumetric energy density of material greater than 200 $kWh \cdot m^{-3}$. A fourth one ($MgCl_2 \cdot 6H_2O$) is added to the previous list if aiming for an effective reduced volumetric energy density of material greater than 100 $kWh \cdot m^{-3}$. It has been reported that this material, often cited as interesting for thermochemical heat storage, cannot be completely dehydrated ($\rightarrow MgCl_2$) solely by heat input (Sharma 2002) and tends to chemically degrade with the formation of HCl (Ferchaud 2016; Sögütoglu et al. 2018).

Reversible (17)		Not promising (28)	
$Al_2(SO_4)_3 \cdot 18H_2O$	$SrBr_2 \cdot 6H_2O$	$AlNH_4(SO_4)_2 \cdot 12H_2O$	$LiBO_2 \cdot xH_2O$
$CaBr_2 \cdot 6H_2O$	$SrCl_2 \cdot 6H_2O$	$BaSO_4 \cdot xH_2O$	$Li(OH) \cdot H_2O$
$CaCl_2 \cdot 6H_2O$	$Zn(NO_3)_2 \cdot 6H_2O$	$Ca(CH_3COO)_2 \cdot xH_2O$	$Li_2SO_4 \cdot H_2O$
$Ce(SO_4)_2 \cdot 4H_2O$		$CaF_2 \cdot xH_2O$	$Mg_3(PO_4)_2 \cdot 8H_2O$
$K_2CO_3 \cdot 1.5H_2O$		$CaSO_4 \cdot 2H_2O$	$NaNO_3 \cdot xH_2O$
$KOH \cdot 2H_2O$		$Cs_2SO_4 \cdot xH_2O$	$Na_2B_4O_7 \cdot 10H_2O$
$LaCl_3 \cdot 7H_2O$		$CsCl \cdot xH_2O$	$NaCH_3COO \cdot 3H_2O$
$La(NO_3)_3 \cdot 6H_2O$		$Fe(NO_3)_3 \cdot 9H_2O$	$Na_2O_4W \cdot 2H_2O$
$LiCl \cdot H_2O$		$K_4[Fe(CN_6)] \cdot 3H_2O$	$Na_2SO_4 \cdot 10H_2O$
$LiNO_3 \cdot 3H_2O$		$K_2OTiO_2 \cdot xH_2O$	$NaHCO_3 \cdot xH_2O$
$MgBr_2 \cdot 6H_2O$		$K_2SO_4 \cdot xH_2O$	$NiNO_3 \cdot 6H_2O$
$MgCl_2 \cdot 6H_2O$		$KAl(SO_4)_2 \cdot 12H_2O$	$Sr(NO_3)_2 \cdot xH_2O$
$MgSO_4 \cdot 7H_2O$		$KBr \cdot xH_2O$	$TiO(SO_4) \cdot xH_2O$
$Na_2S_2O_3 \cdot 5H_2O$		$KCl \cdot xH_2O$	$ZnSO_4 \cdot 7H_2O$

Table 1.8. *Result of the basic thermogravimetric analysis: 17 reversible reactions and 28 non-promising reactions*

Sodium sulfide hydrates ($Na_2S \cdot xH_2O$) are also shown in Figure 1.17, even though they were eliminated in the preliminary selection phase due to their strong toxicity and corrosiveness. These salts are known for their high corrosivity and require relatively severe (low) operating pressures with other issues, such as the formation of H_2S and H_2 vapor (de Jong et al. 2014); it has also been highlighted that in the presence of CO_2 – hence atmospheric air – these materials are entirely unstable and lose their thermochemical qualities (Sögütoglu et al. 2018). However, they offer a high volumetric energy storage density (Figure 1.17), which decreases rapidly with cycles in the presence of CO_2. To use these materials, a pure substance in a hermetically sealed reactor would be required, increasing costs (Sögütoglu et al. 2018).

Since the melting temperature of $Na_2S \cdot 9H_2O$ is 49°C, only $Na_2S \cdot 5H_2O$ could be considered for applications requiring domestic hot water (DHW) production if no techniques are planned to manage the salt's melting.

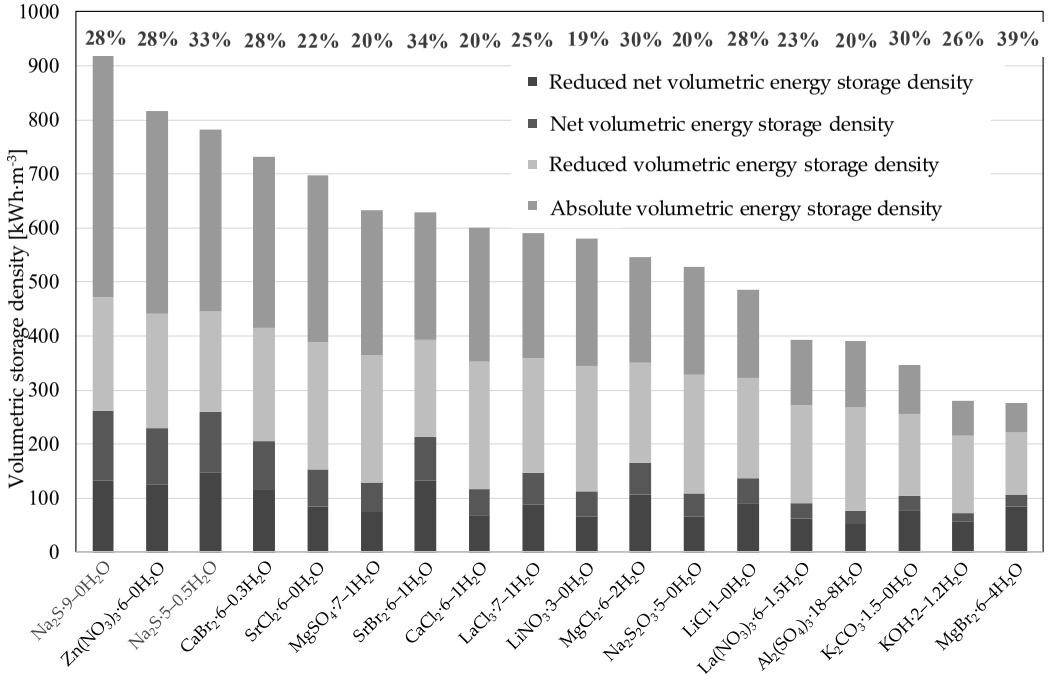

Figure 1.17. *The volumetric energy storage densities and the effective thermal efficiencies η for each of the salts that provide a reversible reaction after dehydration at 105°C in a dry atmosphere. The numbers above the histograms correspond to the thermal efficiency η. For example, for the reaction* $CaCl_2 \cdot 6H_2O + \Delta h_r \rightarrow CaCl_2 \cdot H_2O + 5H_2O$, $\eta = 20\%$; *the absolute volumetric energy density is* $D_V = 601\ kWh \cdot m^{-3}$, *while the reduced effective volumetric energy storage density is* $D^*_{V,net} = 69\ kWh \cdot m^{-3}$. *For a color version of this figure, see www.iste.co.uk/lepierres/heat2.zip*

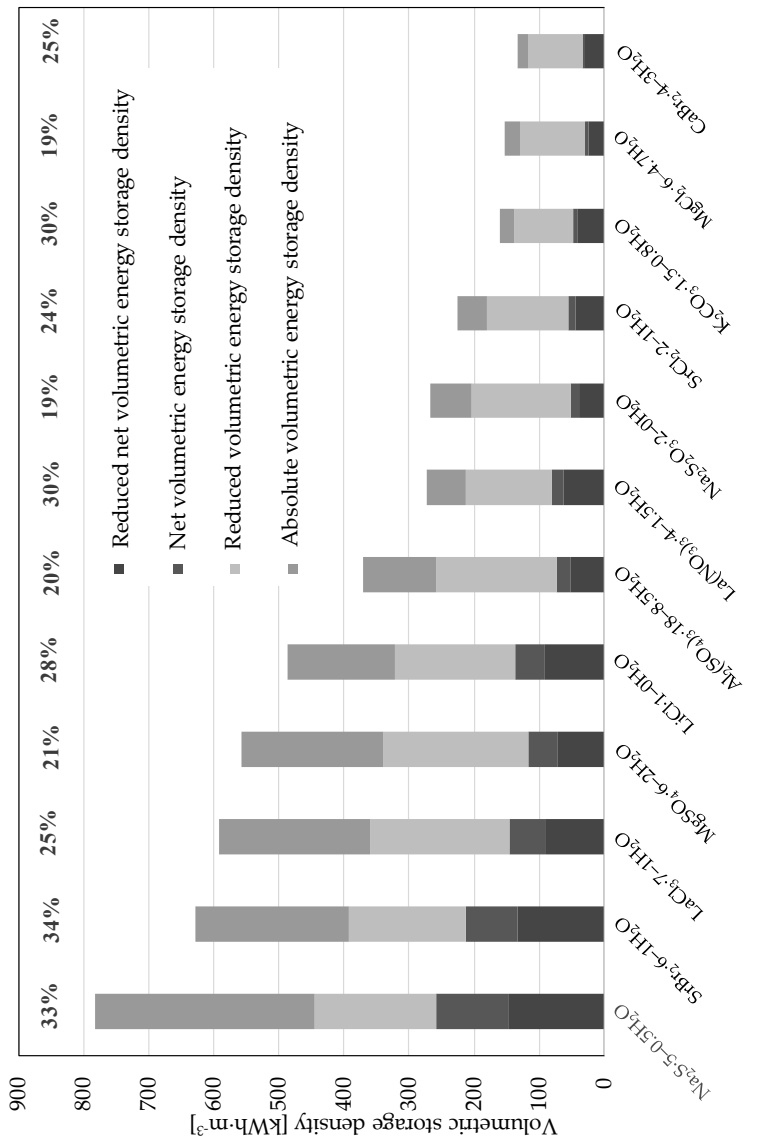

Figure 1.18. *Various volumetric energy densities and thermal efficiency for 11 of the 17 salts offering a reversible reaction after dehydration at 105°C under humid conditions (21 mbar water vapor pressure). For a color version of this figure, see www.iste.co.uk/lepierres/heat2.zip*

Third, a TGA to confirm the dehydration in a humid atmosphere and hydration at 60°C are carried out. The previous 17 materials are now subjected to a TGA under an atmosphere with a water vapor pressure of 21 mbar (equilibrium pressure of the water at 18°C) at 105°C, at a heating rate of 1 $K \cdot min^{-1}$. Only the hydrates with a melting point higher than 60°C are considered at this stage, since the problem of the melting of the salts is not one that is specifically intended to be addressed. The hydrates obtained at the end of the dehydration are then no longer necessarily the same since the atmosphere is no longer dry, reflecting real operating conditions, especially for closed systems. The obtained hydrates, as well the volumetric energy storage densities, are presented in Figure 1.18. There are five salts that have been eliminated at this stage.

According to the data presented in Figure 1.18, the top three salt hydrates are $SrBr_2 \cdot 6H_2O$, $LaCl_3 \cdot 7H_2O$ and $MgSO_4 \cdot 6H_2O$, excluding sodium sulfide, which was eliminated in a previous stage. $SrBr_2 \cdot 6H_2O$ offers the highest values for volumetric energy storage density and thermal efficiency.

The equilibria of the $MgSO_4 \cdot xH_2O$ system are complex, and they are too close to the pure water equilibrium curve. A minimum water vapor pressure of about 150 mbar (equivalent to 54°C at the evaporator) is required to reach 60°C in the reactor. Therefore, this salt is challenging to use, but a better understanding of the $MgSO_4 \cdot xH_2O$ equilibrium system could potentially change this conclusion. $SrBr_2 \cdot 6H_2O$ has already been documented and studied at the prototype scale for various applications. An approximately 80°C temperature is sufficient for complete dehydration, transitioning from hexahydrate to monohydrate. A water vapor pressure greater than 40 mbar (corresponding to water saturation at a temperature of 29°C) is necessary to reach 60°C in the reactor. Although there is no available data on $LaCl_3 \cdot xH_2O$ systems, $LaCl_3 \cdot H_2O$ was subjected to hydration under a water vapor pressure of 21 mbar at 60°C. Under these conditions, hydration led to the formation of $LaCl_3 \cdot 3H_2O$. This salt, which has not been considered for thermochemical heat storage, appears as an interesting candidate for such applications. Further studies could explore its hydration under higher water vapor pressures.

For an application requiring 60°C for discharging temperature, $SrBr_2 \cdot 6H_2O$ and $LaCl_3 \cdot 7H_2O$ emerge as the most promising salts, ignoring their prices. However, the maximum effective reduced volumetric energy density, a criterion used in contexts demanding high efficiency and considering the market value of the involved heat, offered by these two salts

(133 $kWh \cdot m^{-3}$ and 89 $kWh \cdot m^{-3}$, respectively), would likely fall short of the target, namely an effective reduced energy storage density typically set around 100 $kWh \cdot m^{-3}$ for the storage unit. Even for applications requiring a low discharging temperature, for example, 35°C, the achievable effective thermal storage density and thermal efficiency are relatively low. Despite the prevalence of salt hydrates as storage materials, most salts have led to technical performances below expectations, including a discharging temperature, thermal storage density or power density (kinetics) that is too low or insufficient, not to mention stability issues (cyclability).

In her doctoral thesis, Druske (2020) focused on mixtures of multiple salts obtained either by simple physical mixing or by dissolution followed by evaporation/crystallization. The aim was to improve the stability (cyclability) of materials and their energy storage density. Sixty-two mixtures were prepared using sulfates, chlorides and bromides of the following cations: Na^+, K^+, Li^+, Sr^{2+}, CA^{2+}, Mg^{2+}, Zn^{2+}, Fe^{2+}, Fe^{3+} and Al^{3+} (Table 1.9). It is noteworthy that almost all of these salts were individually considered in the study by N'Tsoukpoe et al. (2014b) mentioned earlier.

From this set, only four mixtures ($\{2MgCl_2 + KCl\}$, $\{2MgCl_2 + CaCl_2\}$, $\{5SrBr_2 + 8CaCl_2\}$ and $\{2ZnCl_2 + CaCl_2\}$) were found interesting (high mass energy storage density, stability of the mixture during cycling) following ATG/DSC measurements.

Further studies on a larger scale (recycling from 10–25 cycles of 20–100 g of material) show that only $\{2MgCl_2 + KCl\}$ and $\{2MgCl_2 + CaCl_2\}$ would be feasible for thermochemical heat storage. In the case of $\{2MgCl_2 + CaCl_2\}$, the formation of Mg(OH)Cl and HCl occurs when the temperature exceeds 110°C without affecting the energy storage density. This formation of hydrochloric acid is problematic for the use of the material in thermochemical heat storage. This decomposition is not observed when using $\{2MgCl_2 + KCl\}$ up to a temperature of 200°C.

Overall, in the study, KCl proves to be an interesting stabilizer, although it itself practically does not store heat, which negatively affects the energy storage density. The study did not clearly demonstrate that the mixture could offer a (significantly?) greater thermal storage density than the material originally having the highest energy storage density before the mixture.

Category	Mixtures
Sulfates	{$3Na_2SO_4 + K_2SO_4$}, {$Na_2SO_4 + K_2SO_4$}, {$Na_2SO_4 + 3K_2SO_4$}, {$2Na_2SO_4 + MgSO_4$}, {$7Na_2SO_4 + 4MgSO_4$}, {$2K_2SO_4 + MgSO_4$}, {$7Na_2SO_4 + 4ZnSO_4$}, {$10K_2SO_4 + 7ZnSO_4$}, {$3MgSO_4 + 2ZnSO_4$}, {$Na_2SO_4 + Fe_2 + SO_4$}, {$2Na_2SO_4 + Fe_2 + SO_4$}, {$9K_2SO_4 + 5Fe_2 + SO_4$}, {$2Fe_n(SO_4)_m + Al_2(SO_4)_3$}, {$2Na_2SO_4 + Al_2(SO_4)_3$}, {$17MgSO_4 + 3Al_2(SO_4)_3$}, {$MgSO_4 + Al_2(SO_4)_3$}
Chlorides	{$MgCl_2{\cdot}6H_2O$}, {$CaCl_2{\cdot}2H_2O$}, {$ZnCl_2$}, {KCl}, {$CaCl_2 + 2MgCl_2$}, {$CaCl_2 + MgCl_2$}, {$2CaCl_2 + MgCl_2$}, {$2CaCl_2 + ZnCl_2$}, {$CaCl_2 + ZnCl_2$}, {$CaCl_2 + 2ZnCl_2$}, {$2MgCl_2 + ZnCl_2$}, {$MgCl_2 + ZnCl_2$}, {$MgCl_2 + 2ZnCl_2$}, {$2MgCl_2$ + KCl}, {$MgCl_2$ + KCl}#1, {$MgCl_2$ + KCl}#2, {$MgCl_2$ + 2KCl}, {$2CaCl_2$ + KCl}, {$CaCl_2$ + KCl}, {$CaCl_2$ + 2KCl}, {$8ZnCl_2$ + 7KCl}, {$4ZnCl_2$ + 7KCl}, {$2ZnCl_2$ + 7KCl} {$MgCl_2 + CaCl_2 + ZnCl_2$}, {$MgCl_2 + CaCl_2$ + 2KCl}, {$MgCl_2 + ZnCl_2$ + 2KCl}, {$CaCl_2 + ZnCl_2$ + 2KCl}, {$MgCl_2 + CaCl_2 + ZnCl_2$ + 3KCl}
Bromides	{$SrBr_2{\cdot}6H_2O$}, {NaBr}, {KBr}, {LiBr}, {$MgBr_2{\cdot}6H_2O$}, {$CaBr_2{\cdot}xH_2O$}, {$2NaBr + SrBr_2$}, {$NaBr + SrBr_2$}, {$NaBr + 2SrBr_2$}, {$2KBr + SrBr_2$}, {$KBr + SrBr_2$}, {$KBr + 2SrBr_2$}, {$2LiBr + SrBr_2$}, {$LiBr + SrBr_2$}, {$LiBr + 2SrBr_2$}, {$2MgBr_2 + SrBr_2$}, {$MgBr_2 + SrBr_2$}, {$MgBr_2 + 2SrBr_2$}, {$2CaBr_2 + SrBr_2$}, {$CaBr_2 + SrBr_2$}, {$CaBr_2 + 2SrBr_2$}, {$5CaBr_2 + 4SrBr_2$}, {$5CaBr_2 + 8SrBr_2$}, {$5CaBr_2 + 16SrBr_2$}
Sulfates + Chlorides	{$16KCl + 3MgSO_4$}, {$ZnSO_4 + 36ZnCl_2$}
Sulfates + Bromides	{$4SrBr_2 + 3MgSO_4$}, {$2SrBr_2 + 3MgSO_4$}, {$SrBr_2 + 3MgSO_4$}
Chlorides + Bromides	{$2SrBr_2$ + 5KCl}, {$SrBr_2$ + 5KCl}, {$SrBr_2$ + 10KCl}, {$5SrBr_2 + 4CaCl_2$}, {$5SrBr_2 + 8CaCl_2$}, {$5SrBr_2 + 16CaCl_2$}

Table 1.9. *Complete group of salts and salt mixtures studied by Druske (2020)*

1.5.2.3.2. Materials for thermochemical heat storage at high temperature

Different categories of chemical reactions have been studied for thermochemical heat storage at medium and high temperatures (Table 1.10).

The system of $CaO/Ca(OH)_2$ is by far the one that has attracted the most attention in recent years among the primary systems studied for thermal storage by chemical reactions for temperatures ranging from about 200°C to 600°C, or even higher. By adjusting the water vapor pressure, one can easily modify or control the discharging temperature up to beyond 600°C (Liu et al. 2018). CaO, like MgO, is known to be readily available, non-toxic and inexpensive (Pardo et al. 2014; Liu et al. 2018; Humphries et al. 2019) and the reaction is easy to implement. One of the main challenges with this material remains the issue of particle agglomeration and its low thermal conductivity. Processes involving the use of ammonia are the most mature (Table 1.10), notably because the synthesis of ammonia from nitrogen and hydrogen, which are relatively abundant reactants, is a well-established industrial technique. As it is a gas-phase-only reaction, it exhibits excellent reversibility compared to solid–gas reactions, with both gases being well known and stable within the envisaged temperature range. Moreover, there is no need to store the fluids in separate containers since their densities are significantly different at room temperature and moderate pressure (Liu et al. 2018).

However, the harsh operating conditions, including high pressure and temperature, and safety requirements for gas storage contribute to the high operational cost of using this reaction for heat storage.

The achieved thermal storage energy density in this temperature range could also reach almost 900 $kWh \cdot m^{-3}$ (Table 1.10). However, thermal energy storage density is not necessarily a primary concern for industrial storage. In industrial settings, considerations such as space constraints and availability are different from those in residential areas. The primary concern is whether the reaction is technically feasible at an acceptable cost. Even safety constraints are more manageable here than in residential applications. For instance, ammonia storage is feasible in an industrial context, which is practically impossible for a domestic application, as explained in section 1.5.1.

Reaction category	Reaction	Operating conditions	Storage density
Hydroxides	$Mg(OH)_2 + \Delta H_r \leftrightarrow MgO + H_2O$ (solid–gas)	$T_c = 150°C$ $T_d = 100°C$	388 kWh·m^{-3} 390 kWh·t^{-1}
	$Ca(OH)_2 + \Delta H_r \leftrightarrow CaO + H_2O$ (solid–gas)	$T_c = 450°C$ $T_d = 25–400°C$	437 kWh·m^{-3} 390 kWh·t^{-1}
Hydrides	$MgH_2 + \Delta H_r \leftrightarrow Mg + H_2$ (solid–gas)	$T_c = 380°C$ $T_d = 230°C$	580 kWh·m^{-3} 800 kWh·t^{-1}
	$CaH_2 + \Delta H_r \leftrightarrow Ca + H_2$ (solid–gas)	$T_c = 380°C$ $T_d = 230°C$	580 kWh·m^{-3} 1,071 kWh·t^{-1}
Carbonates	$PbCO_3 + \Delta H_r \leftrightarrow PbO + CO_2$ (solid–gas)	$T_c = 450°C$ $T_d = 300°C$	303 kWh·m^{-3} 90 kWh·t^{-1}
	$CaCO_3 + \Delta H_r \leftrightarrow CaO + CO_2$ (solid–gas)	$T_c = 860°C$ $T_d = 880°C$	692 kWh·m^{-3} 490 kWh·t^{-1}
Ammoniacal solutions	$NH_4HSO_4 + \Delta H_r \leftrightarrow NH_3 + H_2O + SO_3$ (liquid–gas)	$T_c = 927°C$ $T_d = 427°C$	860 kWh·m^{-3} 810 kWh·t^{-1}
	$2NH_3 + \Delta H_r \leftrightarrow N_2 + 2H_2$ (gas)	$T_c = 450°C$ $P_c = 9–150$ bars $T_d = 450°C$ $P_d = 10–300$ bars	745 kWh·m^{-3} 1,090 kWh·t^{-1}

Table 1.10. *Reactions studied for high temperature thermochemical heat storage (Pardo et al. 2014; Humphries et al. 2019). The storage energy density is given relative to the first material in the left side of the equation*

Reaction category	Reaction	Operating conditions	Energy storage density
Redoxes	$2Co_3O_4 + \Delta H_r \leftrightarrow 6CoO + O_2$ (solid–gas)	T = 870–900°C	295 kWh·m^{-3} 240 kWh·t^{-1}
	$2BaO_2 + \Delta H_r \leftrightarrow 2BaO + O_2$ (solid–gas)	T = 690–780°C	328 kWh·m^{-3} 130 kWh·t^{-1}
Organics	$CH_4 + H_2O + \Delta H_r \leftrightarrow 3H_2 + CO$ (gas)	T_c = 950°C T_d = 530°C	7.8 kWh·m^{-3} 4,340 kWh·t^{-1}
	$CH_4 + CO_2 + \Delta H_r \leftrightarrow 2H_2 + 2CO$ (gas)	T_c = 950°C T_d = 530°C	7.7 kWh·m^{-3} 4,280 kWh·t^{-1}
	$C_6H_{12} + \Delta H_r \leftrightarrow C_6H_6 + 3H_2$ (liquid–gas)	T_c = 317°C T_d = 397°C	530 kWh·m^{-3} 680 kWh·t^{-1}
SO_3	$2SO_3 + \Delta H_r \leftrightarrow 2SO_2 + O_2$ (liquid–gas)	T_c = 800°C T_d = 500–600°C	646 kWh·m^{-3} 340 kWh·t^{-1}

Table 1.10. *Reactions studied for high-temperature thermochemical heat storage (Pardo et al. 2014; Humphries et al. 2019). The energy storage density is given relative to the first material on the left side of the equation (continued)*

1.5.2.4. *Coupled chemisorption and physisorption*

Due to various stability issues with materials, several research teams have shifted toward using matrices of physisorbents (typically zeolite or silica gel) that are more stable. These matrices are usually impregnated with salt hydrates. The volumetric energy storage density takes a hit, decreasing by approximately 60–70% (Hongois et al. 2011; Nonnen et al. 2016) for at least two reasons. First, these matrices have a lower volumetric storage energy density compared to the salts. Second, the amount of salt hydrates that can be impregnated to obtain a stable and sufficiently porous material is generally limited (usually 5–20%) (Hongois et al. 2011; Mette et al. 2013; Nonnen et al. 2016). Additionally, depending on operating conditions, the composite material may exhibit a lower energy storage density than each of the individual materials (Whiting et al. 2013; Nonnen et al. 2016). In such cases, the composite material becomes less advantageous, and it is often more practical to use the stable material alone, as seen with certain zeolites (Whiting et al. 2013; Metchueng Kamdem 2016). Zeolites can achieve discharging temperatures suitable for DHW needs, but the required charging temperature is generally higher, exceeding 150°C, and sometimes 250°C. Although it is possible to reduce the charging temperature, it comes at the expense of energy storage density (Lass-Seyoum et al. 2016).

The use of additive materials with no real sorption capacity, especially those intended for improving thermal or mass transfer or maintaining the stability of the active material, is discussed in section 1.6.

1.6. Introduction to the issue of heat and mass transfer in solid–gas storage materials

1.6.1. *Kinetics of the adsorption phenomenon or solid–gas reaction*

Let us consider a fire truck with a full water tank with a capacity of 6 m^3 arriving at a fire. If the opening of the hose connected to the tank can only deliver a flow rate of 15 $L \cdot h^{-1}$, equivalent that of a shower head, there is little chance that the firefighters will be able to put out the flames in time, even though a 6 m^3 capacity would normally be sufficient to extinguish the fire in question. It is not enough to simply have a sufficient water storage that water must also be transferred at a sufficient flow rate. The same is true for thermal energy storage. It is not enough to store a large amount of heat in

a small storage unit: it is also necessary to be able to recover the heat at a rate, or power, sufficient to meet the user's needs. A storage of 1,800 kWh of heat is of little use if, during the cold period when the building requires a power of 1 kW for the comfort of its occupants, the storage can only provide 100 W! A high specific power, meaning the power that can be exchanged with the material per unit mass or volume, is one of the key performance elements of a reactor and, consequently, of a thermochemical heat storage material. Specific power depends, among other things, on the kinetics of the reaction in play. The reaction kinetics in a solid–gas reactor will be presented in more detail in Chapter 3, which is dedicated to reactors. The aim here is to introduce the origin of transfer limitations at the material level and some approaches implemented to reduce these limitations and improve transfers.

Thermal energy storage reactors by sorption or chemical reaction involve coupled heat and mass transfers. Aside from the periods of temperature rise/fall of the material in the reactor, at the beginning or end of operation, any heat transfer in the material is accompanied by gas release/fixation as long as the temperature and pressure conditions allow the sorption phenomenon. The kinetics of the phenomenon in the reactor depends precisely on heat and mass transfers, as well as the *deviation from equilibrium*. The analyses presented in this chapter are generally under the thermodynamic equilibrium conditions of the considered pairs. However, at thermodynamic equilibrium, by definition, the reaction rate is zero, and nothing happens. For example, when two identical pieces of copper at the same temperature are in thermal contact, nothing happens, as the potential for transfer, here at the temperature, is the same. In contrast, when one of the two pieces is initially at a higher temperature than the other, heat transfer is observed between the two pieces until thermal equilibrium is reached. This transfer decreases, that is, it becomes less and less rapid, with the decrease in temperature difference between the two pieces. Similarly, in a thermochemical reactor, the reaction kinetics are faster when the deviation from equilibrium conditions, or deviation from equilibrium, is large. This can be, for example, a difference in pressure or temperature. Thus, a sufficiently high water vapor pressure for discharging (lower for charging) is necessary to achieve a sufficient reaction kinetics (Rambaud 2009; Michel 2012; Michel et al. 2012; Richter et al. 2018).

Adsorbents are used in the form of powders, pellets, granules or beads. These forms and sizes of the material will influence not only the energy storage density but also important aspects such as mass and heat transfer

within the material. Adsorbents are, by definition, porous materials; they generally exhibit low thermal conductivity (Table 1.11). This low thermal conductivity, coupled with that of the gaseous sorbate filling the pores, especially at low pressure (Table 1.11), and the low thermal contacts between solid grains due to intergranular discontinuity/porosity, leads to a relatively low overall heat transfer in the reactor, primarily occurring through conduction across the material bed (Figure 1.19). Furthermore, the decomposition reaction, for example, dehydration of a salt hydrate, is accompanied by a decrease in the volume of the salt grain, while the synthesis reaction, for example, hydration, is accompanied by an increase in the volume of the salt grain. These volume variations lead to modifications, particularly those of the texture and porosity of the material, significantly affecting heat transfers within the material.

Mass transfer, or gas diffusion into the material, depends, among other factors, on permeability, which is a measure of the ability of a porous material to be "passed through" by a fluid. This mass transfer is generally poor in low-pressure processes due to the low pressure of the gaseous phase. One of the phenomena frequently observed in thermochemical reactors using chemisorbents, generally salt hydrates and hydroxides, is the decrease in the permeability of the material after a few cycles, that is, a succession of decomposition and synthesis reactions. This decrease in permeability is related to agglomeration of solid particles in the reactor. It may be just the formation of a surface crust that prevents vapor from diffusing and accessing the grains available under the crust. One can think of the formation of a crust on a pile of powdered sugar deposited in a relatively humid place. It can also be a mass uptake of the entire material. This is the example of quicklime powder deposited in a pile in a humid outdoor environment: one obtains a more or less hard block. Sometimes, the loss of permeability is the result of solidification following a more or less accidental melting of the material when its melting temperature is locally reached (see Box 1.1).

The loss of permeability can also be due to "overhydration": the salt or part of the salt, typically the surface layer, absorbs too much water, forming a paste or even a solution. The subsequent dehydration of this paste can lead to an increase in the compactness of the material. This happens with highly deliquescent materials, such as calcium chloride ($CaCl_2 \cdot nH_2O$). In any case, regardless of the origin of the loss or reduction in permeability, the result is the same: the gas (sorbate) no longer accesses the entire solid material, and the reaction becomes impossible. This is one of the main limitations of using chemisorbents.

Material	Form	Thermal conductivity [$W \cdot m^{-1} \cdot K^{-1}$]
Zeolite	Solid grain Granular bed Granular bed (H_2O)	0.18–0.4 0.03–0.15 0.03–0.15
Activated carbon	Solid grain Granular bed Granular bed (methanol)	0.54 0.3–0.5 0.14–0.17
Silica gel	Solid grain Granular bed Granular bed (H_2O)	0.37–0.8 0.05–0.20 0.04–0.26
$CaCl_2$	Granular bed	0.1–0.2
$Ca(OH)_2$	Granular bed	0.1
Water vapor	Vapor (6–100 mbar)	0.016–0.020

Table 1.11. *Thermal conductivity of various materials (solid grains) and effective thermal conductivity of unconsolidated beds (granular beds) (N'Tsoukpoe et al. 2014a)*

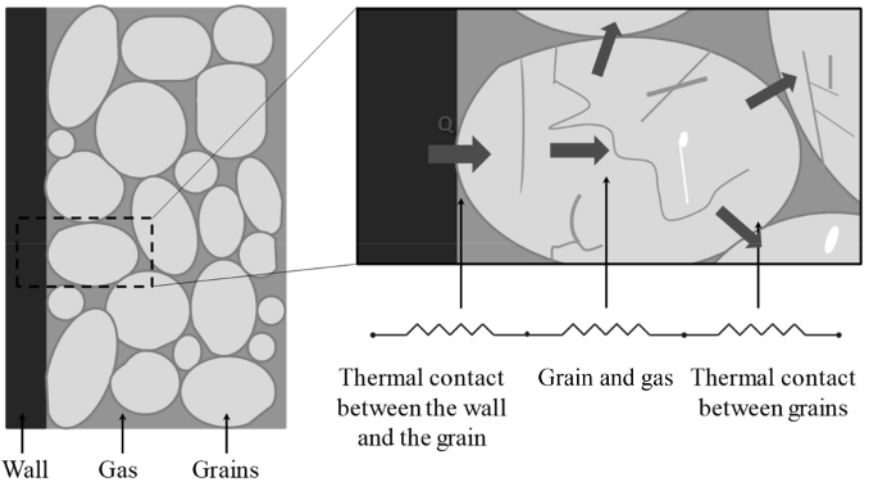

Figure 1.19. *Thermal resistances along the thermal transfer path in a porous bed with a heat exchanger (N'Tsoukpoe et al. 2014a). For a color version of this figure, see www.iste.co.uk/lepierres/heat2.zip*

$Na_2S·9H_2O$ is a salt that can release up to 9 moles of water per mole of salt, which means that in principle it offers a high volumetric energy storage density. This is also the case if we consider the reaction $Na_2S·9H_2O + \Delta H_r \leftrightarrow Na_2S + 9H_2O$, which offers an energy storage density of 924 $kWh·m^{-3}$ for $Na_2S·9H_2O$, one of the highest among all salt hydrates (Figure 1.17). However, the melting temperature of $Na_2S·9H_2O$ is 49°C. It has been observed that when the rate of heating of the material in a reactor or in a calorimeter exceeds 1.6 $K·min^{-1}$, the complete dehydration of the $Na_2S·9H_2O$ does not have time to occur before the temperature reaches 49°C (this temperature needs to be exceeded to obtain Na_2S under the operating conditions). Consequently, partial or almost total melting of the material occurs, accompanied by a modification of its structure that hinders or limits subsequent hydrations (de Boer et al. 2002). Thus, depending on the rate of heating or temperature rise of the material, the partial or total melting of the material occurs instead of dehydration. This can lead to the destruction of the structure of the material and result in particle agglomeration.

For use requiring the production of domestic hot water, only $Na_2S·5H_2O$ (with a melting temperature of 83°C) is considered if there are no planned techniques to manage the melting of the salt using the reaction $Na_2S·5H_2O + \Delta H_r \leftrightarrow Na_2S·0.5H_2O + 4.5H_2O$. Even in this case, the melting of the $Na_2S·5H_2O$ is observed under a heating rate of 1.6 $K·min^{-1}$ when exceeding 83°C in the presence of water vapor.

During the hydration phase $Na_2S·2H_2O + 3H_2O \rightarrow Na_2S·5H_2O + \Delta H_r$, which can achieve a temperature of 60°C for a water evaporation temperature of about 10°C, the formation and fusion of $Na_2S·9H_2O$ can be observed, while all of $Na_2S·2H_2O$ has not yet become $Na_2S·5H_2O$.

All of these factors make the use of Na_2S hydrates challenging, as it requires specific operating conditions and precautions to harness their significant volumetric energy density for storage, not to mention other problems mentioned in section 1.5.2. Similar issues exist for other highly hydrated salts with a relatively low melting temperature, such as $AlNH_4(SO_4)_2·12H_2O$ or $KAl(SO_4)_2·12H_2$ (Galwey and Brown 1999; Marias et al. 2014; N'Tsoukpoe et al. 2014b).

Box 1.1. *Na_2S hydrates melting issues*

1.6.2. *Improvements to the characteristics of thermochemical heat storage materials*

According to Rambaud (2009), the agglomeration of salt grains occurs during synthesis reactions carried out under conditions close to thermodynamic equilibrium, especially when these are not far from the salt dissolution conditions (saturated solution). Consequently, a proper determination of the implementation conditions of the reaction could avoid the formation of agglomerates. However, researchers often opt for another approach: dispersing the salt in a more stable material (Table 1.12). One of the most commonly used matrices for this purpose is vermiculite. Others use more stable physisorbents, such as silica gel or zeolite (Figure 1.20), as matrices, allowing them to benefit from the sorption capacity of these materials.

The main technique used to immobilize the salt in the matrix pores is impregnation. It involves first drying the matrix to remove any absorbed water before impregnating the matrix particles in an aqueous solution of the salt (Gordeeva et al. 2013). Any excess solution that is not fixed in the matrix pores is removed either by filtration or by vacuum drying. The amount of salt that can be fixed in the matrix pores without encountering the formation of agglomerates again is relatively limited, significantly affecting the volumetric energy storage density.

In different studies (Hongois 2011; Marias 2015), the composites do not exhibit more than 20–40% of their absolute volumetric energy storage density, not forgetting that the bonding energy could also decrease due to the physisorbents (section 1.5.2.4). It is possible that some salt hydrates melt but regain their original structure, especially if they are inserted into another stable matrix, as seems to be the case with $CaCl_2$ confined in silica gel (Aristov et al. 1996). It is also observed that the material resulting from the impregnation of a salt (monovariant equilibrium) into the pores of a physisorbent (divariant equilibrium) can follow a monovariant equilibrium (Gordeeva et al. 2013), but this does not seem to always be the case (Hongois 2011).

As for improving heat transfer, various techniques are employed, such as adding metallic or carbon fibers to the material. In the case of carbon fibers, a consolidated material is typically produced, meaning a compact solid structure. This tends to reduce permeability, and the choice of matrix, as well

as the implementation, is carried out to ensure and preserve minimal porosity. One of the most commonly used carbon materials is expanded natural graphite (ENG). It is a material with a very low apparent density (~3–4 $kg \cdot m^{-3}$), high intrinsic thermal conductivity (~200 $W \cdot m^{-1} \cdot K^{-1}$), significant porosity, and good elasticity (Stitou 2013). The resulting consolidated composite material has high porosity (60–90%) and high effective thermal conductivity (5–40 $W \cdot m^{-1} \cdot K^{-1}$), depending on the apparent density of ENG in the composite material (~50–200 $kg \cdot m^{-3}$). Increasing the amount of ENG thus increases thermal conductivity, favouring heat transfer in the material but reducing its permeability, which hinders mass transfer (Figure 1.21). The choice of the amount of ENG to implement depends on the requirements of the intended application.

For thermochemical heat storage, it is clear that the amount of ENG should be kept minimal to maximize thermal energy storage density. Because long-term thermochemical heat storage requires a significant amount of material, corresponding to a low average volumetric power requirement, some authors argue that the use of graphite in this context is not justified (Stitou 2013; Michel et al. 2014). This requirement for low volumetric power is indeed low if one considers that the entire material in the storage is subjected to the reaction simultaneously, as suggested by Michel et al. (2014): for a storage system involving 5–10 t of $SrBr_2 \cdot 6H_2O$, the authors estimate it at 0.3–0.8 $W \cdot kg^{-1}$ by dividing the required thermal power (3–4 kW) by the total mass of the storage material. However, the assumption of the simultaneous reaction of all storage material, that is, several tons of salt, is generally not adopted in the literature, explaining the use of carbon materials, even for long-term thermal energy storage (Table 1.12).

The use of composite materials is becoming increasingly systematic in the case of solid sorbents, with porous matrices, especially zeolites, being employed to disperse and stabilize the medium while taking advantage of their storage capacity. This provides the opportunity to lower the charging temperature while modifying the sorption characteristics to adapt to operating conditions. The main drawback of these materials remains the reduction in volumetric energy storage density and the decrease in the temperature of heat release for the same water vapor pressure.

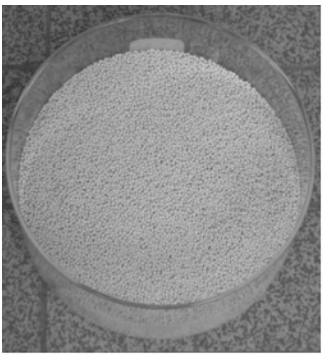

Zeolite

$MgSO_4$

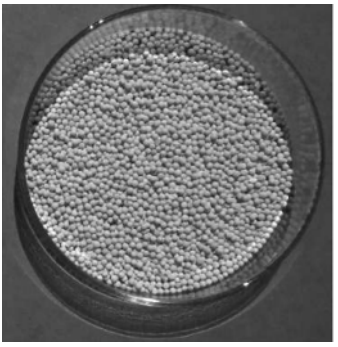

Composite of Zeolite-$MgSO_4$

Figure 1.20. *Zeolite 13X, $MgSO_4$ and zeolite-$MgSO_4$ composite with a mass fraction of 15% of $MgSO_4$ (Hongois 2011). For a color version of this figure, see www.iste.co.uk/lepierres/heat2.zip*

Matrix	Salt	Comments	References
Attapulgite	$CaCl_2$ (30 m%)	–	(Jänchen et al. 2005)
Attapulgite	$MgSO_4$, $MgSO_4$ + $MgCl_2$	Mixtures of salt in different proportions, use of impregnation techniques to increase the energy storage density and heat transfers	(Posern and Kaps 2010)
Aluminosilicate	$CaCl_2$	–	(Jänchen et al. 2004)
Bentonite	$CaCl_2$ (40 m%)	Impregnation, maximum energy storage density of the composite material: 185 $kWh \cdot m^{-3}$	(Kerskes et al. 2010)
Expanded natural graphite (ENG)	$CaCl_2$	–	(Tian et al. 2012)
Activated carbon, silica gel, zeolite, vermiculite	$CaCl_2$, $MgSO_4$, $Ca(NO_3)_2$, $Li(NO_3)_2$, LiBr	–	(Casey et al. 2014)
Activated carbon	$CaCl_2$	–	(Casey et al. 2014)
Activated carbon fiber	$CaCl_2$	–	(Druske et al. 2014)
γ-Alumina 'IK-02-200'	$CaCl_2$	–	(Gordeeva et al. 1998)
Carbon sibunit	LiBr	–	(Gordeeva et al. 2002)
Activated carbon/silica gel	$CaCl_2$	–	(Tso and Chao 2012)
Alumina	$CaCl_2$	–	(Tanashev et al. 2013)
Silica-alumina	$CaCl_2$, $Ba(OH)_2$, $LiNO_3$	–	(Jabbari-Hichri et al. 2015)
Mesoporous silica gel	$CaCl_2$	–	(Aristov et al. 1996)
Silica gel	$CaCl_2$, $MgSO_4$, $Ca(NO_3)_2$, $Li(NO_3)_2$, LiBr	–	(Casey et al. 2014)
Microporous silica gel	$Ca(NO_3)_2$	–	(Simonova et al. 2009)

Matrix	Salt	Comments	References
KSK silica gel	$CaCl_2$, $MgCl_2$, LiBr	–	(Tanashev et al. 2013)
Silica gel	$CaCl_2$	–	(Wu et al. 2007)
Silica gel	LiCl	–	(Gordeeva et al. 2009)
Silica gel	$MgSO_4$	–	(Aristov and Gordeeva 2009)
Silica gel	$NaSO_4$	–	(Aristov and Gordeeva 2009)
Silica gel	$Ca(NO_3)_2$	–	(Simonova et al. 2009)
Ordered iron silicate matrix and disordered iron silicate matrix	$CaCl_2$ (7m%)	–	(Ristić and Henninger 2014)
Expanded natural graphite	$CaCl_2$, $SrCl_2$, $BaCl_2$–$FeCl_3$, $NiCl_2$, $MnCl_2$–NH_4Cl, NaBr	–	(Jiang et al. 2013)
Impacted expanded natural graphite ENGB and expanded natural graphite powder ENGP	$CaCl_2$ + KCl	–	(Druske et al. 2014)
Graphite	$SrBr_2$	–	(Lahmidi et al. 2006)
Zeolite 13X	$MgSO_4$	Tests on 200 g of the composite material ZM15 (zeolite 13X impregnated with 15% by mass of $MgSO_4$), charging: 150°C; discharging: 30°C; energy storage density of the composite material: 166 $kWh \cdot m^{-3}$	(Hongois 2011; Hongois et al. 2011)
Zeolite 13X	$CaCl_2$, $MgSO_4$, $Ca(NO_3)_2$, $Li(NO_3)_2$, LiBr	–	(Casey et al. 2014)

Matrix	Salt	Comments	References
Vermiculite	$CaCl_2$, $MgSO_4$, $Ca(NO_3)_2$, $Li(NO_3)_2$, LiBr	–	(Casey et al. 2014)
Vermiculite and zeolite	$CaCl_2$	–	(Aydin et al. 2016)
Vermiculite	$CaCl_2$	–	(Aristov et al. 2000)
Vermiculite	$LiNO_3$	–	(Sapienza et al. 2012)
MCM-41	$CaCl_2$	–	(Tokarev et al. 2002)
MCM-41 and SBA-15	3, 5 and 7% of Al_3SO_4	–	(Jabbari-Hichri et al. 2016)
Vermiculite	$SrBr_2$	–	(Zhang et al. 2016)
Wakkanai siliceous shale (WSS)	$CaCl_2$	–	(Liu et al. 2013)
WSS	LiCl	–	(Liu et al. 2015)

Table 1.12. *Various composite materials studied for thermochemical heat storage (N'Tsoukpoe 2012b; Marias 2015; Jarimi et al. 2019)*

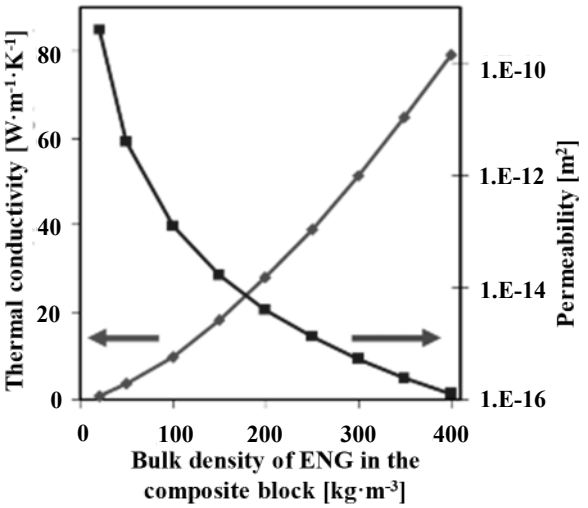

Figure 1.21. *Evolution of effective thermal conductivity and permeability of a reactive composite block as a function of the bulk density of ENG (Stitou 2013). For a color version of this figure, see www.iste.co.uk/lepierres/heat2.zip*

1.7. Overview of material characterization for thermochemical heat storage applications

This section aims to provide an overview of the main material characterization techniques used by research teams focusing on thermochemical heat storage applications. Techniques specifically related to porous materials (porosity measurement, particle size distribution, etc.) are not extensively discussed here. An overview is provided in Table 1.13. Readers interested in these aspects may find useful information in the IUPAC document on key methods for characterizing porous materials (Rouquerol et al. 1994).

Thermal scientists typically seek information that helps specify the thermodynamic conditions for using the material and estimate the energy storage density. This primarily involves determining the thermodynamic equilibrium conditions of the material and estimating the enthalpies of the phenomena.

1.7.1. *Determination of thermodynamic equilibrium conditions*

For solid–gas chemical reactions, one of the initial experimental approaches is the use of TGA to verify if the reaction can occur under the envisaged thermodynamic conditions, such as the sorbate vapor pressure and temperature of the heat source during charging, and the sorbate vapor pressure and temperature during discharging.

TGA also helps determine the stoichiometry of the reaction and its potential steps. It provides an indication of the reversibility of the reaction. TGA is a thermal analysis method that involves tracking the mass evolution of a material sample during heating, cooling, or constant temperature holding under a specified atmosphere. The analyzer includes a highly sensitive balance, a temperature-controlled furnace, a unit for evacuating and controlling the atmosphere, and a data control and recording system. A small amount of material (approximately 10 mg) is deposited in an inert crucible and placed on the analyzer's highly sensitive balance (Figure 1.22).

	Normal
Gas adsorption	Only measures the open pores Pore size: 0.4–50 nm Easy Proven technique
Mercury porosimetry	Similar to the gas adsorption technique Only measures the open pores Pore size > 1.5 nm Easy Proven technique
Transmission electron microscopy (TEM)	Provides information on pore connectivity The size of the pores can be measured if the material contains ordered pores Rarely used for pore analysis
Scanning electron microscopy (SEM)	Pore size > 5 nm Rarely used for pore analysis
Small angle X-ray scattering (SAXS)	All pore sizes Open and closed porosity
Small angle neutron scattering (SANS)	All pore sizes Open and closed porosity Expensive

Table 1.13. *Various techniques for characterizing porous materials*

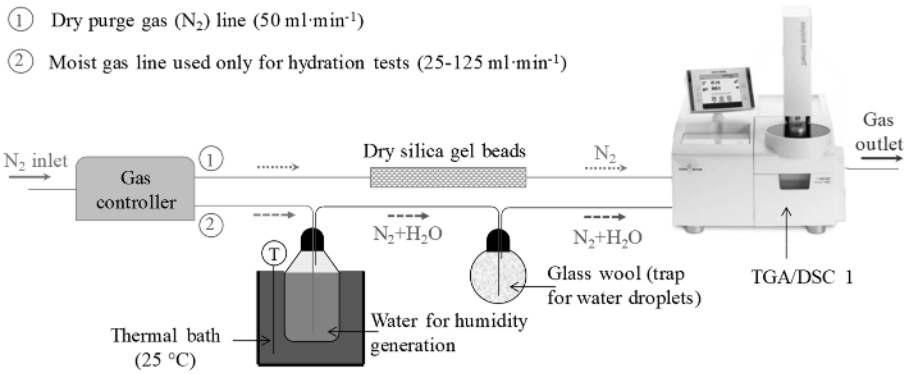

Figure 1.22. *Example of an experimental setup for thermogravimetric analysis (N'Tsoukpoe et al. 2014b). For a color version of this figure, see www.iste.co.uk/lepierres/heat2.zip*

The sample undergoes a temperature variation using a typically inert gas (e.g., nitrogen, helium, or argon) following a predefined program. A temperature probe in direct contact with the crucible allows monitoring the exact temperature of the sample, while its mass is continuously recorded by the electronic balance. Box 1.2 presents an example of TGA results. Interested readers may refer to relevant articles on the subject in the Techniques de l'Ingénieur (Daudon 2001; Wirth et al. 2014).

When it is determined that the material meets a minimum set of criteria, a setup can be arranged to determine a few points on the equilibrium curve of water vapor pressure as a function of temperature.

Figure 1.24 illustrates a device used for characterizing the equilibrium reactions of salt hydrates at low temperatures. In principle, a quantity of salt arranged in a thin layer comes into contact with the vapor phase of the sorbate, which is vaporized at a given temperature using another thermostat bath. The entire system, being previously evacuated by a vacuum pump, has a vapor pressure equal to the saturation pressure of the sorbate at the temperature set by the thermostat bath. This allows for varying the sorbate pressure and measuring the temperature evolution in the salt bed. Of course, it is necessary to allow a "sufficiently long" time for equilibrium to be established, meaning there is no significant temperature variation in the salt bed over a defined period.

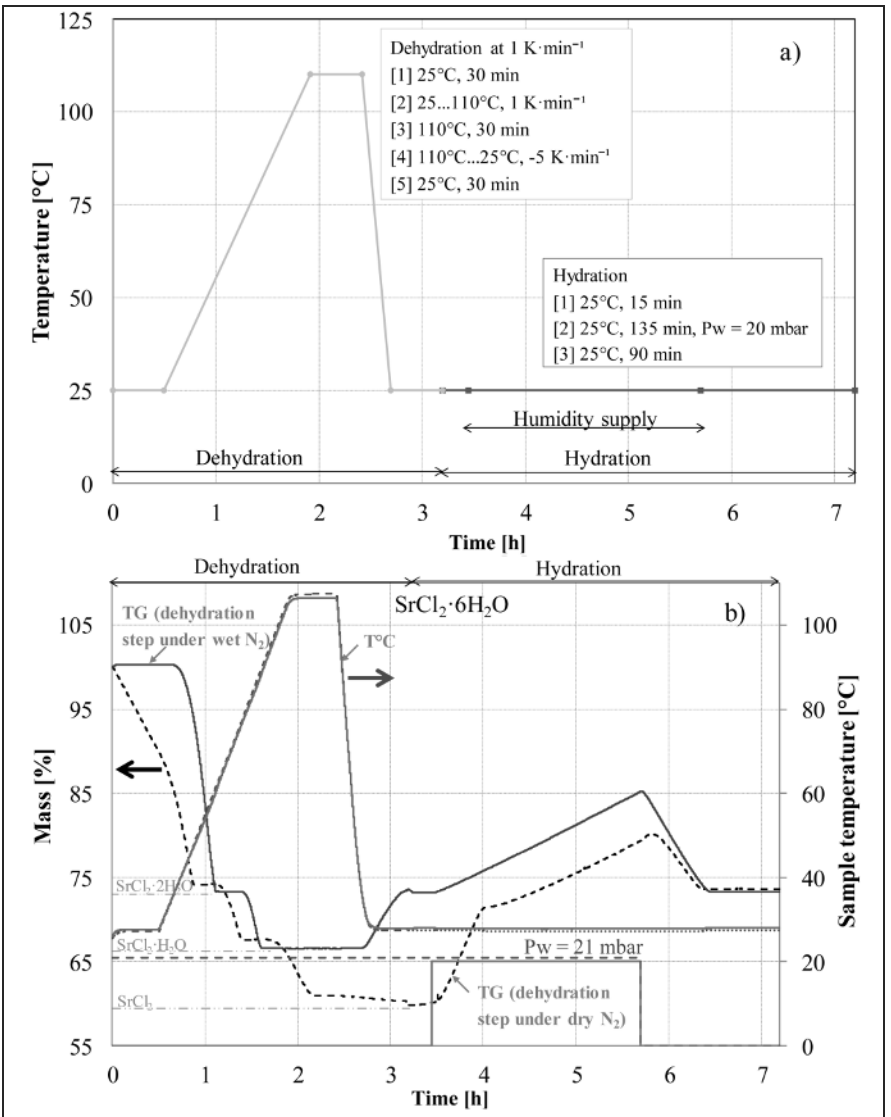

Figure 1.23. *Thermogravimetric analysis of $SrCl_2 \cdot 6H_2O$ (N'Tsoukpoe et al. 2014b). For a color version of this figure, see www.iste.co.uk/lepierres/heat2.zip*

Figure 1.23(b) presents a thermogram of $SrCl_2 \cdot 6H_2O$ subjected to a two-step program (Figure 1.23(a)). In the first step, the material is exposed to a stream of dry nitrogen with a temperature increase from 25°C to approximately 110°C at a

heating rate of 1 $K \cdot min^{-1}$. This is followed by a plateau of half an hour at 110°C before the sample is cooled back to 25°C to be exposed to a stream of humid nitrogen with a water vapor pressure of 20 mbar, while maintaining the temperature at 25°C.

The first step allows the observation of the dehydration of $SrCl_2 \cdot 6H_2O$ in three consecutive stages: it first loses 4 moles of water ($SrCl_2 \cdot 6H_2O \rightarrow SrCl_2 \cdot 2H_2O + 4H_2O$), then one mole ($SrCl_2 \cdot 2H_2O \rightarrow SrCl_2 \cdot H_2O + H_2O$) and another mole ($SrCl_2 \cdot H_2O \rightarrow SrCl_2 + H_2O$). The material then begins to react with water when humid nitrogen is introduced into the unit. The process is relatively slow, and when the supply of water vapor is suspended after about 2 h, the salt loses water to stabilize as $SrCl_2 \cdot 2H_2O$.

When the same experiment is conducted by introducing humid nitrogen (water vapor: 20 mbar) into the system from the beginning, dehydration at 110°C leads to the formation of $SrCl_2 \cdot H_2O$, and the final dehydration does not occur.

In conclusion, $SrCl_2 \cdot 6H_2O$ can be completely dehydrated at a temperature below 110°C in the absence of water vapor, for example, with dry air. However, if the operation is carried out under humid air or in a closed system with a condensation pressure of 21 mbar (= condensation temperature of 18°C), the monohydrate ($SrCl_2 \cdot H_2O$) is obtained. Since the experiment was stopped before the end of hydration, no definitive conclusion can be drawn regarding the total reversibility of the reaction under the operating conditions, although the trend of the curve suggests it.

Box 1.2. *Example of thermogravimetric analysis results*

With an aqueous solution, a specially designed device can be used, as presented by Nasirzadeh et al. (2004), allowing the measurement of vapor pressures of aqueous solutions over a wide temperature range (25–200°C) with high pressure precision (±0.3 Pa). Alternatively, vapor pressure analyzers, such as ERAVAP, can be used, as employed by Lefebvre (2015) (Figure 1.25).

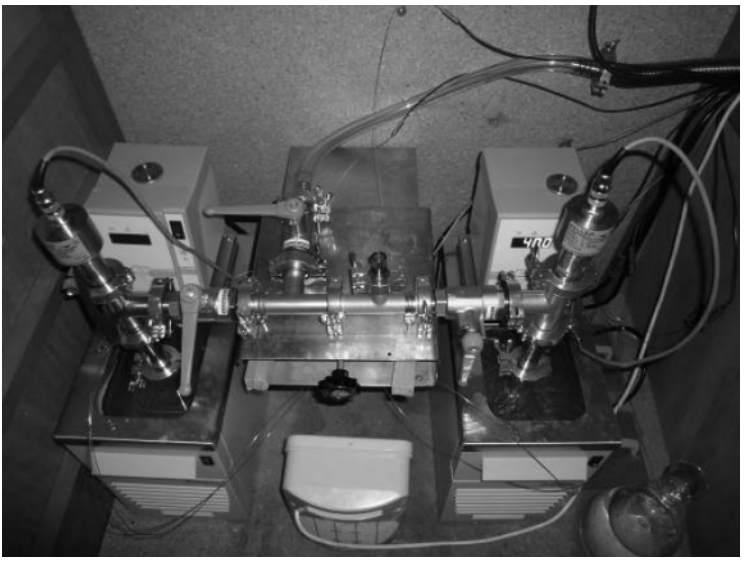

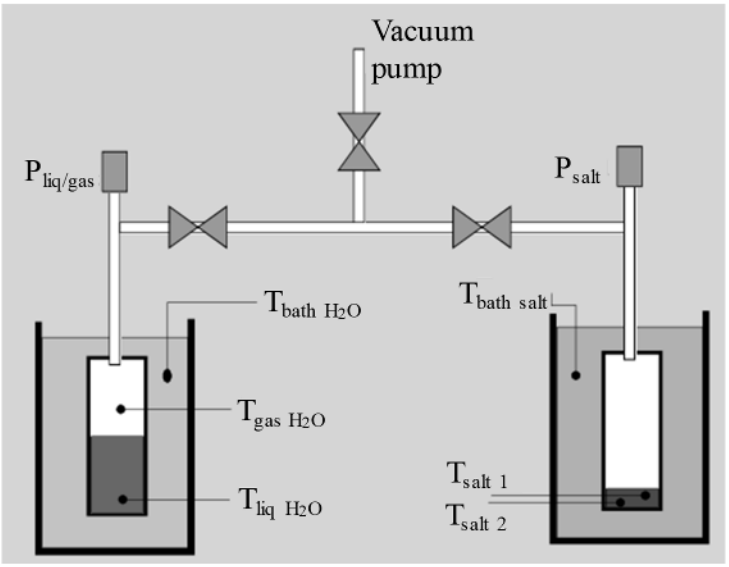

Figure 1.24. *Experimental setup for the characterization of low-temperature reaction equilibria of hydrated salts (Stitou 2013). For a color version of this figure, see www.iste.co.uk/lepierres/heat2.zip*

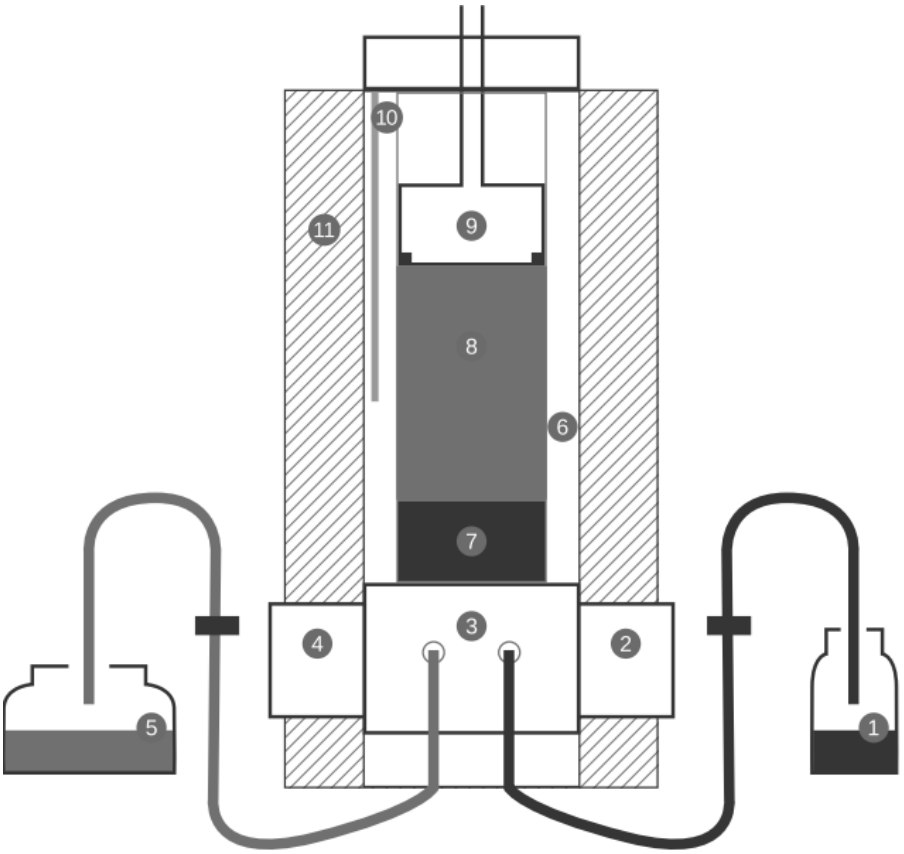

Figure 1.25. *ERAVAP vapor pressure measurement device. 1: sample; 2: inlet valve; 3: manifold; 4: outlet valve; 5: waste container; 6: measuring cell; 7: liquid phase; 8: gas phase; 9: piston with pressure sensor; 10: temperature sensor; 11: insulation (eralytics n.d.)*

For each concentration of the solution to be measured for vapor pressure, a sample is transferred to the measuring cell using a piston by suction after passing through a filter that retains solid particles (undissolved crystals, insoluble particles, etc.). The solution is then brought to the desired measurement temperature. The pressure above the solution is measured by a pressure sensor, and the stabilized value is recorded. Measuring the pressure at three vapor/liquid ratios allows the calculation of the partial pressure of

gases dissolved in the solution (especially air) and the deduction of the vapor pressure of the solution. The temperature of the solution is then raised to obtain another measurement point. When finished with a given concentration, the cells are washed multiple times, including with the new solution of different concentration to be measured.

The results obtained by this method by Lefebvre et al. (2014) are shown in Figure 1.26.

For solid–gas physisorbents, there are various methods for determining adsorption isotherms, with the most common being volumetric and gravimetric methods. Other methods include chromatographic techniques, frequency response techniques, closed-loop recycle, column dynamic and isotope exchange (Auerbach et al. 2003; Sircar and Myers 2003). Gravimetric methods appear more realistic and reliable but are relatively slow compared to volumetric methods.

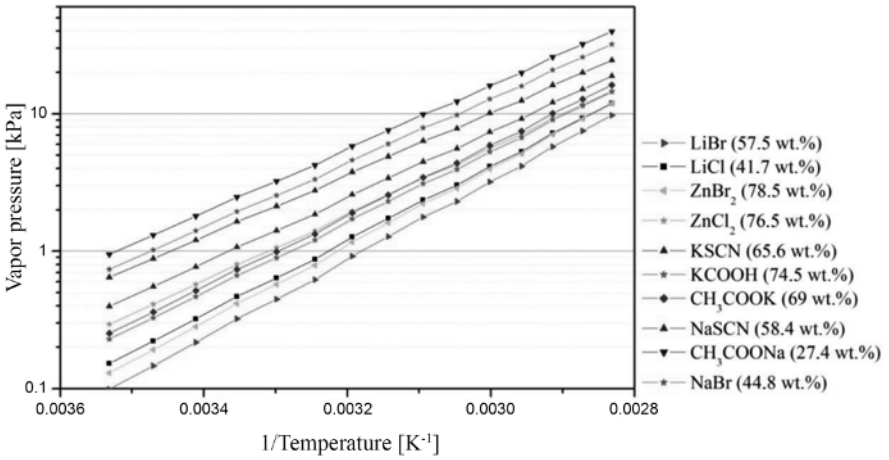

Figure 1.26. *Vapor pressure as a function of the reciprocal of the absolute temperature of aqueous solutions at various mass fractions (Lefebvre et al. 2014). For a color version of this figure, see www.iste.co.uk/lepierres/heat2.zip*

Figure 1.27 presents the principle of these two families of methods. For volumetric methods, the gas pressure is measured before and after expansion of the gas between volumes V_1 and V_2. For the gravimetric method, the mass

of the sample is measured with a magnetic suspension balance when raising the pressure. The second orange-coloured mass in the diagram is used to determine both the gas density and to account for buoyancy. The volume of the sample, in red, must be known in both cases. For more details, one can refer to Appendix 1 of Stadie's (2013) doctoral thesis. These experimental data are then correlated by mathematical models that should best represent the experimental adsorption isotherms (Sun et al. 2016). It is desirable for the models to have both physical significance, consistency with fundamental thermodynamic laws, and numerical processing convenience, which can be very useful when simulating adsorption processes.

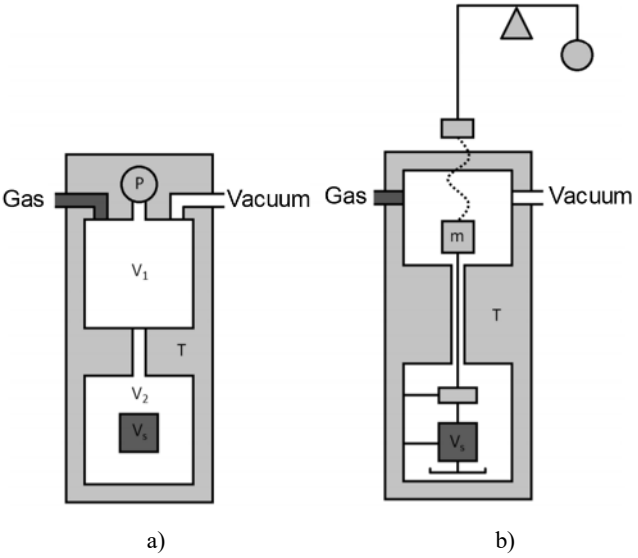

Figure 1.27. *Schematic diagram of the apparatus for determining sorption isotherms using the (a) volumetric and (b) gravimetric methods (Stadie 2013). For a color version of this figure, see www.iste.co.uk/lepierres/heat2.zip*

1.7.2. *Determination of enthalpies*

The determination of enthalpies involves calorimetry, and calorimeters are the main equipment to be used here. For chemical reactions, especially those involving salt hydrates or hydroxides, DSC is the primary technique used. It is generally coupled with TGA, and many microcalorimeters offer

this dual functionality. A crucible containing the sample is subjected to a temperature program simultaneously with an empty crucible, called a reference, in the same chamber. The chamber is therefore heated or cooled at a constant rate, which varies the temperatures of the sample and the reference. The heat flow at the sample is then proportional to the temperature difference between the sample and the ambient temperature (inside the chamber). The same applies to the reference. For more details, see Mehling and Cabeza (2008) or Grenet and Legendre (2010). The analysis of the thermal flux exchanged by the sample allows the detection of any thermal event that occurs during heating/cooling, as well as the evaluation of the amount of heat involved in this event. An example of a result from DSC is provided in Box 1.3.

Figure 1.28 presents the results obtained from a TGA coupled with a DSC. It involves an initial sample of 11.11 mg of a highly hydrated salt subjected to a five-step program:

1) holding temperature at 25°C for 30 min;

2) heating at a constant rate of 1 $K \cdot min^{-1}$ from 25 to 75°C;

3) holding temperature at 75°C for 60 min;

4) cooling at a constant rate of 10 $K \cdot min^{-1}$ from 75 to 55°C;

5) holding at 25°C for 30 min.

The constant-rate heating starts at t = 30 min and ends at t = 80 min, while the phase where the temperature is held constant ends at t = 140 min. It can be observed that the material loses mass from the beginning of heating, accompanied by heat absorption reaching its peak at around the 74th min. The chemical reaction seems to be completed around t = 110 min and corresponds to a mass loss estimated at 4.0447 mg. The integration of the heat flux corresponding to this mass loss is 12.6 J, giving the enthalpy associated with the observed reaction, that is, 1134 $J \cdot g^{-1}$. It should be noted that this is a quick assessment, and repetition of experiments is often useful for a good estimation of the quantities involved (see Figure 1.28).

Box 1.3. *Example of a differential scanning calorimetry result*

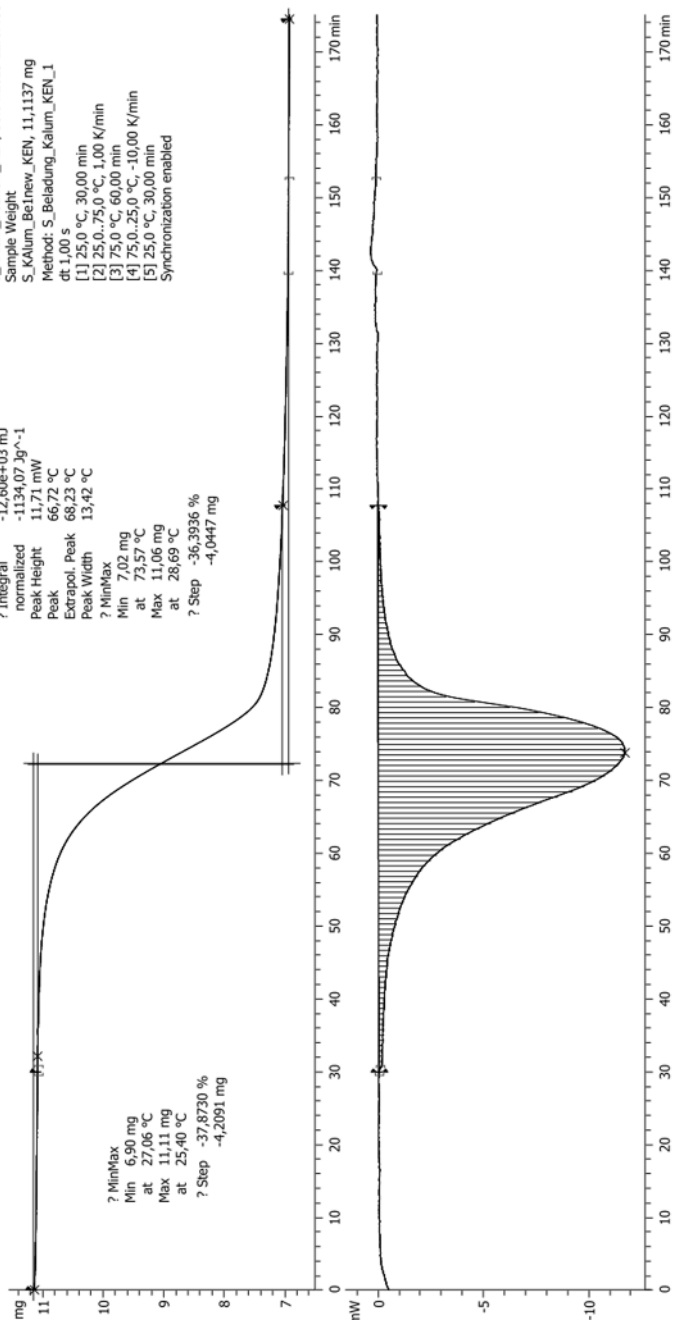

Figure 1.28. *Results of a TGA/DSC of a high salt hydrate*

1.8. References

Adegoke, C.O. (1993). Solubility of the water-lithium-bromide-zinc-bromide combination. *International Journal of Refrigeration*, 16(1), 45–48.

Adokou, K.R.E. (2020). Mise en place d'une bibliothèque de propriétés de matériaux de sorption et identification de matériaux de sorption localement disponibles. Master's Thesis, Institut International d'Ingénierie de l'Eau et de l'Environnement, Ouagadougou.

Alam, K.C.A., Saha, B.B., Akisawa, A., Kashiwagi, T. (2004). Influence of design and operating conditions on the system performance of a two-stage adsorption chiller. *Chemical Engineering Communications*, 191(7), 981–997.

Anies, G. (2011). Modélisation, simulation dynamique, validation expérimentale et optimisation énergétique d'une unité de rafraîchissement solaire par absorption. PhD Thesis, Université de Pau et des Pays de l'Adour, Pau.

Aristov, Y.I. (2007). Novel materials for adsorptive heat pumping and storage: Screening and nanotailoring of sorption properties. *Journal of Chemical Engineering of Japan*, 40(13), 1242–1251.

Aristov, Y.I. and Gordeeva, L.G. (2009). "Salt in a porous matrix" adsorbents: Design of the phase composition and sorption properties. *Kinetics and Catalysis*, 50(1), 65–72.

Aristov, Y.I., Tokarev, M.M., Cacciola, G., Restuccia, G. (1996). Selective water sorbents for multiple applications, 1. $CaCl_2$ confined in mesopores of silica gel: Sorption properties. *Reaction Kinetics and Catalysis Letters*, 59(2), 325–333.

Aristov, Y.I., Restuccia, G., Tokarev, M.M., Buerger, H.D., Freni, A. (2000). Selective water sorbents for multiple applications. 11. $CaCl_2$ confined to expanded vermiculite. *Reaction Kinetics and Catalysis Letters*, 71(2), 377–384.

Auerbach, S.M., Carrado, K.A., Dutta, P.K. (2003). *Handbook of Zeolite Science and Technology*. CRC Press, Boca Raton.

Aydin, D., Casey, S.P., Chen, X., Riffat, S. (2016). Novel "open-sorption pipe" reactor for solar thermal energy storage. *Energy Conversion and Management*, 121, 321–334.

Baerlocher, C., McCusker, L.B., Allen, D.H., Structure Commission of the International Zeolite Association. (2007). *Atlas of Zeolite Framework Types*. Elsevier, Amsterdam [Online]. Available at: www.iza-structure.org/books/Atlas_6ed.pdf [Accessed 2 September 2020].

Bales, C. (2005). Chemical and sorption storage. Selection of concepts. Report B1 of Subtask B, IEA Solar Heating and Cooling Programme [Online]. Available at: http://archive.iea-shc.org/publications/downloads/task32-Chemical_and_Sorption_Storage.pdf [Accessed 4 April 2014].

Bales, C. (2008). Final report of Subtask B. "Chemical and sorption storage". The overview. Report, IEA Solar Heating and Cooling Programme [Online]. Available at: www.iea-shc.org.

Bales, C., Gantenbein, P., Hauer, A., Henning, H.M., Jaenig, D., Kerskes, H., Núñez, T., Visscher, K. (2005). Thermal properties of materials for thermo-chemical storage of solar heat. Report B2 of Subtask B, IEA Solar Heating and Cooling Programme, Borlänge [Online]. Available at: www.iea-shc.org/publications/downloads/task32-Thermal_Properties_of_Materials.pdf.

Bales, C., Gantenbein, P., Jähnig, D., Kerskes, H., Summer, K., van Essen, M., Weber, R. (2008). Laboratory tests of chemical reactions and prototype sorption storage units. Report B4 of Subtask B, IEA Solar Heating and Cooling Programme [Online]. Available at: www.iea-shc.org.

Batten, S.R., Champness, N.R., Chen, X.M., Garcia-Martinez, J., Kitagawa, S., Öhrström, L., O'Keeffe, M., Paik Suh, M., Reedijk, J. (2013). Terminology of metal-organic frameworks and coordination polymers (IUPAC Recommendations 2013). *Pure and Applied Chemistry*, 85(8), 1715–1724.

de Boer, R., Haije, W.G., Veldhuis, J.B.J. (2002). Determination of structural, thermo-dynamic and phase properties in the Na_2S–H_2O system for application in a chemical heat pump. *Thermochimica Acta*, 395(1/2), 3–19.

de Boer, R., Smeding, S.F., Zondag, H.A., Krol, G. (2014). Development of a prototype system for seasonal solar heat storage using an open sorption process. In *Eurotherm Seminar 99: Advances in Thermal Energy Storage*, Lérida [Online]. Available at: www.ecn.nl/publicaties/PdfFetch.aspx?nr=ECN-M–14-009.

Casey, S.P., Elvins, J., Riffat, S., Robinson, A. (2014). Salt impregnated desiccant matrices for 'open' thermochemical energy storage. Selection, synthesis and characterisation of candidate materials. *Energy and Buildings*, 84, 412–425.

Chan, C.W., Ling-Chin, J., Roskilly, A.P. (2013). A review of chemical heat pumps, thermodynamic cycles and thermal energy storage technologies for low grade heat utilisation. *Applied Thermal Engineering*, 50(1), 1257–1273.

Chou, I.M. and Seal, R.R. (2003). Determination of epsomite-hexahydrite equilibria by the humidity-buffer technique at 0.1 MPa with implications for phase equilibria in the system $MgSO_4$-H_2O. *Astrobiology*, 3(3), 619–630.

Darchy, B., Lacour, S., Le Mière, E., Bavoux, E., Domart, Y. (1997). Inhalation de vapeurs d'ammoniaque: valeur pronostique des lésions cutanées. *Réanimation Urgences*, 6(4), 465–469.

Daudon, J.L. (2001). Thermogravimétrie. *Techniques de l'Ingénieur*, P1260 v2, 1–21. doi: 10.51257/a-v2-p1260.

Dicaire, D. and Tezel, F.H. (2009). Study of adsorbent energy density and regeneration for long term thermal energy storage of solar and waste heat. In *Proceedings of the 11th International Conference on Thermal Energy Storage (Effstock 2009)*, Stockholm.

Dicaire, D. and Tezel, F.H. (2011). Regeneration and efficiency characterization of hybrid adsorbent for thermal energy storage of excess and solar heat. *Renewable Energy*, 36, 986–992.

Dirksen, J.A., Ring, T.A., Duvall, K.N., Jongen, N. (2001). Testing of crystallization inhibitors in industrial LiBr solutions. *International Journal of Refrigeration*, 24, 856–859.

Donkers, P.A.J., Sögütoglu, L.C., Huinink, H.P., Fischer, H.R., Adan, O.C.G. (2017). A review of salt hydrates for seasonal heat storage in domestic applications. *Applied Energy*, 199, 45–68.

Druske, M.M. (2020). The reaction of mixed salts in advanced heat storage systems. PhD Thesis, Université Leuphana, Lüneburg [Online]. Available at: https://pubdata.leuphana.de/frontdoor/deliver/index/docId/999/file/The_Reaction_of_Mixed_Salts_in_Advanced_Heat_Storage_Systems.pdf [Accessed 2 September 2020].

Druske, M.M., Fopah-Lele, A., Korhammer, K., Rammelberg, H.U., Wegscheider, N., Ruck, W., Schmidt, T. (2014). Developed materials for thermal energy storage: Synthesis and characterization. *Energy Procedia*, 61, 96–99.

Dyer, A. (2001). Zeolites. In *Encyclopedia of Materials: Science and Technology*, Buschow, K.H.J., Cahn, R.W., Flemings, M.C., Ilschner, B., Kramer, E.J., Mahajan, S., Veyssière, P. (eds). Elsevier, Amsterdam [Online]. Available at: http://www.sciencedirect.com/science/article/pii/B0080431526017848.

Eralytics Eravap (2020). L'analyseur de pression vapeur [Online]. Available at: eralytics.com/wp-content/uploads/1612_eravap_bro_FRANCAIS_web.pdf [Accessed 17 June 2020].

Ferchaud, C.J. (2016). Experimental study of salt hydrates for thermochemical seasonal heat storage. PhD Thesis, Eindhoven University of Technology [Online]. Available at: https://research.tue.nl/files/20452083/20160420_Ferchaud.pdf.

Fernández, R., Ortiz, C., Chacartegui, R., Valverde, J.M., Becerra, J.A. (2019). Dispatchability of solar photovoltaics from thermochemical energy storage. *Energy Conversion and Management*, 191, 237–246.

Fischer, H.R. (2009). What is the best possible heat storage density for a seasonal adsorptive thermal energy storage. In *Proceedings of the 11th International Conference on Thermal Energy Storage (Effstock 2009)*, Stockholm [Online]. Available at: intraweb.stockton.edu/eyos/energy_studies/content/docs/effstock09/posters/163.pdf.

Fumey, B., Weber, R., Gantenbein, P., Daguenet-Frick, X., Williamson, T., Dorer, V. (2014). Closed sorption heat storage based on aqueous sodium hydroxide. *Energy Procedia*, 48, 337–346.

Gaeini, M., Javed, M.R., Ouwerkerk, H., Zondag, H.A., Rindt, C.C.M. (2017). Realization of a 4kW thermochemical segmented reactor in household scale for seasonal heat storage. *Energy Procedia*, 135, 105–114.

Galwey, A.K. and Brown, M.E. (1999). *Thermal Decomposition of Ionic Solids: Chemical Properties and Reactivities of Ionic Crystalline Phases*. Elsevier Science, Amsterdam.

Gantenbein, P. (2008). Fundamental geometrical system structure limitations in a closed adsorption heat storage system. In *Proceedings of the 1st International Conference on Solar Heating, Cooling and Buildings (Eurosun 2008)*, Lisbon.

Gantenbein, P., Brunold, S., Flückiger, F., Frei, U. (2022). Sorption materials for application in solar heat energy storage. Report, Institute für Solartechnik SPF, Université technique de Rapperswil, Rapperswil [Online]. Available at: www.solarenergy.ch.

Gartler, G., Jähnig, D., Purkarthofer, G., Wagner, W. (2004). Development of a high energy density sorption storage system. *Proceedings of Eurosun 2004* [Online]. Available at: aee-intec.at.

Gordeeva, L.G., Tokarev, M.M., Parmon, V.N., Aristov, Y.I. (1998). Selective water sorbents for multiple application, 6. Freshwater production from the atmosphere. *Reaction Kinetics and Catalysis Letters*, 65(1), 153–159.

Gordeeva, L.G., Restuccia, G., Freni, A., Aristov, Y.I. (2002). Water sorption on composites “LiBr in a porous carbon”. *Fuel Processing Technology*, 79(3), 225–231.

Gordeeva, L.G., Freni, A., Aristov, Y.I., Restuccia, G. (2009). Composite sorbent of methanol “lithium chloride in mesoporous silica gel” for adsorption cooling machines: Performance and stability evaluation. *Industrial & Engineering Chemistry Research*, 48(13), 6197–6202.

Gordeeva, L.G., Grekova, A., Krieger, T., Aristov, Y.I. (2013). Composites "binary salts in porous matrix" for adsorption heat transformation. *Applied Thermal Engineering*, 50(2), 1633–1638.

Grenet, J. and Legendre, B. (2010). Analyse calorimétrique différentielle à balayage (DSC). *Techniques de l'Ingénieur*, P1205 v1 [Online]. Available at: https://www.techniques-ingenieur.fr/base-documentaire/mesures-analyses-th1/methodes-thermiques-d-analyse-42384210/analyse-calorimetrique-differentielle-a-balayage-dsc-p1205/.

Grevel, K.D. and Majzlan, J. (2009). Internally consistent thermodynamic data for magnesium sulfate hydrates. *Geochimica et Cosmochimica Acta*, 73(22), 6805–6815.

Hadorn, J.C., Bales, C., Streicher, W., Drueck, H. (2007). Projet 32: Concepts de stockage innovants pour bâtiments solaires et basse énergie. *IEA SHC e-Newsletter*, 4.

Hafida, E.H. (2008). Élaboration et caractérisation de solides microporeux de type MeAPO4-5 et MeAPO4-11 (Me: Fe, Co et Sn). PhD Thesis, Université Abdelhamid Ibn Badis Mostaganem, Mostaganem [Online]. Available at: http://e-biblio.univ-mosta.dz/handle/123456789/955 [Accessed 8 December 2020].

Hauer, A. (2002a). Assessment of solid adsorbents in open sorption systems for energetic applications. PhD Thesis, Technical University of Berlin [Online]. Available at: https://depositonce.tu-berlin.de//handle/11303/766 [Accessed 3 August 2018].

Hauer, A. (2002b). Thermal energy storage with zeolite for heating and cooling applications. In *3rd Workshop of Annex 17 ECES IA/IEA, Advanced Thermal Energy Storage through Phase Change Materials and Chemical Reactions – Feasibility Studies and Demonstration Projects*, Tokyo.

Hauer, A. (2007a). Adsorption systems for TES-Design and demonstration projects. In *NATO Science Series*, Paksoy, H.Ö. (ed.). Springer, Dordrecht [Online]. Available at: www.springerlink.com/content/r78t5x6kn885735t/.

Hauer, A. (ed.) (2007b). Sorption theory for thermal energy storage. In *Thermal Energy Storage for Sustainable Energy Consumption*, Paksoy, H.O. (ed.). Springer, Dordrecht, 393–408.

Hauer, A. (2010). Compact thermal storages: Potentials and limitations for different applications. In *Proceedings of the 2nd International Conference on Solar Heating, Cooling and Buildings (Eurosun 2010)*, San Francisco.

van Helden, W. and Rommel, M. (2015). Compact thermal energy storage: Material development for system integration. IEA SHC Position Paper, Task 42 (ECES Annex 29) [Online]. Available at: www.iea-shc.org/Data/Sites/1/publications/IEA-SHC-Compact-Thermal-Storage-Position-Paper.pdf [Accessed 30 December 2020].

Hiu, L., N'Tsoukpoe, K.E., Le Pierres, N., Luo, L. (2011). Evaluation of a seasonal storage system of solar energy for house heating using different absorption couples. *Energy Conversion and Management*, 52(6), 2427–2436.

Hiu, L., Nagano, K., Sugiyama, D., Togawa, J., Nakamura, M. (2013). Honeycomb filters made from mesoporous composite material for an open sorption thermal energy storage system to store low-temperature industrial waste heat. *International Journal of Heat and Mass Transfer*, 65, 471–480.

Hiu, L., Nagano, K., Togawa, J. (2015). A composite material made of mesoporous siliceous shale impregnated with lithium chloride for an open sorption thermal energy storage system. *Solar Energy*, 186–200.

Hongois, S. (2011). Stockage de chaleur inter-saisonnier par voie thermochimique pour le chauffage solaire de la maison individuelle. PhD Thesis, Institut National des Sciences Appliquées, Lyon.

Hongois, S., Kuznik, F., Stevens, P., Roux, J.J. (2011). Development and characterisation of a new $MgSO_4$-zeolite composite for long-term thermal energy storage. *Solar Energy Materials and Solar Cells*, 95(7), 1831–1837.

Humphries, T.D., Møller, K.T., Rickard, W.D.A., Sofianos, M.V., Liu, S., Buckley, C.E., Paskevicius, M. (2019). Dolomite: A low cost thermochemical energy storage material. *Journal of Materials Chemistry A*, 7(3), 1206–1215.

International Union of Pure and Applied Chemistry (2014). Compendium of chemical terminology: Gold book. Report, International Union of Pure and Applied Chemistry, Oxford.

Jabbari-Hichri, A., Bennici, S., Auroux, A. (2015). Enhancing the heat storage density of silica–alumina by addition of hygroscopic salts ($CaCl_2$, $Ba(OH)_2$, and $LiNO_3$). *Solar Energy Materials and Solar Cells*, 140, 351–360.

Jabbari-Hichri, A., Bennici, S., Auroux, A. (2016). Effect of aluminum sulfate addition on the thermal storage performance of mesoporous SBA-15 and MCM-41 materials. *Solar Energy Materials and Solar Cells*, 149, 232–241.

Jähnig, D., Hausner, R., Wagner, W., Isaksson, C. (2006). Thermo-chemical storage for solar space heating in single-family house. In *Proceedings of the 10th International Conference on Thermal Energy Storage, Ecostock 2006*, New Jersey.

Jänchen, J., Ackermann, D., Stach, H., Brösicke, W. (2004). Studies of the water adsorption on zeolites and modified mesoporous materials for seasonal storage of solar heat. *Solar Energy*, 76(1/3), 339–344.

Jänchen, J., Ackermann, D., Weiler, E., Stach, H., Brösicke, W. (2005). Calorimetric investigation on zeolites, $AlPO_4$'s and $CaCl_2$ impregnated attapulgite for thermochemical storage of heat. *Thermochimica Acta*, 434(1/2), 37–41.

Jarimi, H., Aydin, D., Yanan, Z., Ozankaya, G., Chen, X., Riffat, S. (2019). Review on the recent progress of thermochemical materials and processes for solar thermal energy storage and industrial waste heat recovery. *International Journal of Low-Carbon Technologies*, 14(1), 44–69.

Jiang, L., Wang, L.W., Jin, Z.Q., Wang, R.Z., Dai, Y.J. (2013). Effective thermal conductivity and permeability of compact compound ammoniated salts in the adsorption/desorption process. *International Journal of Thermal Sciences*, 71, 103–110.

de Jong, A.J., Trausel, F., Finck, C., van Vliet, L., Cuypers, R. (2014). Thermochemical heat storage – System design issues. *Energy Procedia*, 48, 309–319.

Kerskes, H. (2006). Seasonal sorption heat storage. In *Danvak seminar (Solar heating systems - Combisystems - Heat storage)*, DTU Lyngby.

Kerskes, H., Asenbeck, S., Mette, B., Bertsch, F., Müller-Steinhagen, H. (2010). Experimental and numerical investigations on thermo-chemical heat storage. In *Proceedings of the 2nd International Conference on Solar Heating, Cooling and Buildings (Eurosun 2010)*, Graz [Online]. Available at: task42.iea-shc.org/data/sites/1/publications/Task42-Experimental_and_Numerical_Investi-gations_on_Thermo-Chemical_Heat_Storage.pdf [Accessed 14 September 2014].

Krese, G., Kozelj, R., Butala, V., Stritih, U. (2018). Thermochemical seasonal solar energy storage for heating and cooling of buildings. *Energy & Buildings*, 164, 239–253.

Lahmidi, H., Mauran, S., Goetz, V. (2006). Definition, test and simulation of a thermochemical storage process adapted to solar thermal systems. *Solar Energy*, 80(7), 883–893.

Lass-Seyoum, A., Borozdenko, D., Friedrich, T., Langhof, T., Mack, S. (2016). Practical test on a closed sorption thermochemical storage system with solar thermal energy. *Energy Procedia*, 91, 182–189.

Le Pierrès, N. (2014). Procédés à sorption pour la conversion, le stockage et le transport de l'énergie thermique : du matériau à l'intégration énergétique du procédé. HDR, Université de Grenoble, Grenoble.

Lee, H.R., Koo, K.K., Jeong, S., Kim, J.S., Lee, H., Oh, Y.S., Park, D.R., Baek, Y.S. (2000). Thermodynamic design data and performance evaluation of the water + lithium bromide + lithium iodide + lithium nitrate + lithium chloride system for absorption chiller. *Applied Thermal Engineering*, 20(8), 707–720.

Lefebvre, E. (2015). Procédé par absorption avec stockage d'énergie solaire intersaisonnier intensifié par la cristallisation de l'absorbant : recherche & caractérisation thermodynamique de nouveaux couples; conception de la cuve de stockage. PhD Thesis, Université de Lyon 1, Lyon.

Lefebvre, E., Gagnière, E., Bennici, S., Auroux, A., Mangin, D. (2014). Étude des propriétés thermodynamiques de solutions salines dans le cadre d'un procédé de stockage inter-saisonnier de l'énergie solaire. In *Actes du Congrès de la Société Française de Thermique*, Lyon [Online]. Available at: www.sft.asso.fr/Local/sft/dir/user-3775/documents/actes/Congres_2014/Communi-cations/8836.pdf [Accessed 24 August 2018].

Leppäjärvi, T., Malinen, I., Kangas, J., Tanskanen, J. (2012). Utilization of P_i^{sat} temperature-dependency in modelling adsorption on zeolites. *Chemical Engineering Science*, 69(1), 503–513.

Liu, D., Xin-Feng, L., Bo, L., Si-quan, Z., Yan, X. (2018). Progress in thermochemical energy storage for concentrated solar power: A review. *International Journal of Energy Research*, 42(15), 4546–4561.

Marias, F.E. (2015). Analyse, conception et expérimentation de procédés de stockage thermique résidentiel de longue durée par réaction thermochimique à pression atmosphérique. PhD Thesis, Université Grenoble Alpes, Grenoble [Online]. Available at: https://tel.archives-ouvertes.fr/tel-01207191/document [Accessed 5 September 2018].

Marias, F.E., Neveu, P., Tanguy, G., Papillon, P. (2014). Thermodynamic analysis and experimental study of solid/gas reactor operating in open mode. *Energy*, 66, 757–765.

Mauran, S., Lahmidi, H., Goetz, V. (2008). Solar heating and cooling by a thermochemical process. First experiments of a prototype storing 60 kWh by a solid/gas reaction. *Solar Energy*, 82(7), 623–636.

Mehling, H. and Cabeza, L.F. (2008). *Heat and Cold Storage with PCM. An Up To Date Introduction into Basics and Applications*. Springer-Verlag, Berlin.

Metchueng Kamdem, S. (2016). Stockage de chaleur dans l'habitat par sorption zéolithe/H_2O. PhD Thesis, Université de Lyon, Lyon [Online]. Available at: theses.insa-lyon.fr/publication/2016LYSEI059/these.pdf [Accessed 8 May 2018].

Mette, B., Kerskes, H., Drück, H., Badenhop, T., Salg, F., Gläser, R. (2013). Thermochemical energy storage as an element for the energy turnaround. In *Proceedings of the 8th International Renewable Energy Storage Conference and Exhibition (IRES 2013)*, Berlin.

Michel, B. (2012). Procédé thermochimique pour le stockage intersaisonnier de l'énergie solaire : modélisation multi-échelles et expérimentation d'un prototype sous air humide. PhD Thesis, Université de Perpignan Via Domitia, Perpignan.

Michel, B., Mazet, N., Mauran, S., Stitou, D., Xu, J. (2012). Thermochemical process for seasonal storage of solar energy: Characterization and modeling of a high density reactive bed. *Energy*, 47(1), 553–563.

Michel, B., Mazet, N., Neveu, P. (2014). Experimental investigation of an innovative thermochemical process operating with a hydrate salt and moist air for thermal storage of solar energy: Global performance. *Applied Energy*, 129, 177–186.

Mugnier, D. (2013). Market available chillers for solar cooling. *Solar Update*, 57, 12.

Nasirzadeh, K., Zimin, D., Neueder, R., Kunz, W. (2004). Vapor-pressure measurements of liquid solutions at different temperatures: Apparatus for use over an extended temperature range and some new data. *Journal of Chemical & Engineering Data*, 49(3), 607–612.

Nicolas, S., Lopez, K., Lutz, C., Bouvier, L. (2015). Zéolithes à porosité hiérarchisée. Patent, WO2015019013A2 [Online]. Available at: https://patents.google.com/patent/WO2015019013A2/fr.

Nonnen, T., Beckert, S., Gleichmann, K., Brandt, A., Unger, B., Kerskes, H., Mette, B., Bonk, S., Badenhop, T., Salg, F., Gläser, R. (2016). Expérimentation d'un stockage thermochimique à long terme à base d'un composite zéolithe-sel. *Chemie Ingenieur Technik*, 88(3), 363–371.

N'Tsoukpoe, K.E. (2012). Étude du stockage à long terme de l'énergie solaire thermique par procédé d'absorption LiBr–H_2O pour le chauffage de l'habitat. PhD Thesis, Université de Grenoble, Le Bourget du Lac [Online]. Available at: https://tel.archives-ouvertes.fr/tel-00710249.

N'Tsoukpoe, K.E. (2018). Énergie solaire thermique : production, utilisation et rationalisation de la gestion. HDR, Université Grenoble Alpes, Grenoble.

N'Tsoukpoe, K.E. and Kuznik, F. (2021). A reality check on long-term thermochemical heat storage for household applications. *Renewable and Sustainable Energy Reviews*, 139, 110683.

N'Tsoukpoe, K.E., Le Pierrès, N., Luo, L. (2012). Numerical dynamic simulation and analysis of a lithium bromide/water long-term solar heat storage system. *Energy*, 37(1), 346–358.

N'Tsoukpoe, K.E., Restuccia, G., Schmidt, T., Py, X. (2014a). The size of sorbents in low pressure sorption or thermochemical energy storage processes. *Energy*, 77, 983–998.

N'Tsoukpoe, K.E., Schmidt, T., Rammelberg, H.U., Watts, B.A., Ruck, W.K.L. (2014b). A systematic multi-step screening of numerous salt hydrates for low temperature thermochemical energy storage. *Applied Energy*, 124, 1–16.

N'Tsoukpoe, K.E., Osterland, T., Opel, O., Ruck, W.K.L. (2016). Cascade thermochemical storage with internal condensation heat recovery for better energy and exergy efficiencies. *Applied Energy*, 181, 562–574.

Office fédéral de l'environnement (2015). Installations de réfrigération: Prudence avec l'ammoniac [Online]. Available at: https://www.bafu.admin.ch/bafu/fr/home/themen/thema-stoerfallvorsorge/stoerfaelle–dossiers/stoerfallvorsorge–kaelteanlagen-mit-ammoniak–sicherheit-ist-ei.html [Accessed 5 May 2020].

Pardo, P., Deydier, A., Anxionnaz-Minvielle, Z., Rougé, S., Cabassud, M., Cognet, P. (2014). A review on high temperature thermochemical heat energy storage. *Renewable and Sustainable Energy Reviews*, 32, 591–610.

Pataskar, S.G., Adyanthaya, S.D., Devotta, S., Holland, F.A. (2011). Performance of an experimental absorption heat transformer using aqueous lithium bromide, lithium chloride, and lithium bromide/lithium chloride solutions. *Industrial & Engineering Chemistry Research*, 29, 1658–1662.

Patek, J. and Klomfar, J. (2006). A computationally effective formulation of the thermodynamic properties of LiBr–H_2O solutions from 273 to 500 K over full composition range. *International Journal of Refrigeration*, 29, 566–578.

Payra, P. and Dutta, P.K. (2003). Zeolites: A primer. In *Handbook of Eolite Science and Technology*, Auerbach, S.M., Carrado, K.A., Dutta, P.K. (eds). CRC Press, Boca Raton.

Posern, K. and Kaps, C. (2010). Calorimetric studies of thermochemical heat storage materials based on mixtures of $MgSO_4$ and $MgCl_2$. *Thermochimica Acta*, 502(1), 73–76.

Rambaud, G. (2009). Problématique des transferts en milieu poreux réactif déformable pour procédés de rafraîchissement solaire. PhD Thesis, Université de Perpignan, Perpignan.

Rao, N.K., Hanson, J., Dulloo, M.E., Ghosh, K., Nowell, A., Larinde, M. (2006). Manual of seed handling in genebanks. Report, Bioversity International, Rome [Online]. Available at: www.bioversityinternational.org/fileadmin/user_upload/online_library/publications/pdfs/1167.pdf.

Rathgeber, C., Lävemann, E., Hauer, A. (2015). Economic top–down evaluation of the costs of energy storages – A simple economic truth in two equations. *Journal of Energy Storage*, 2, 43–46.

Rathgeber, C., Hiebler, S., Lävemann, E., Dolado, P., Lazaro, A., Gasia, J., de Gracia, A., Miró, L., Cabeza, L.F., König-Haagen, A. et al. (2016). IEA SHC Task 42/ECES Annex 29 – A simple tool for the economic evaluation of thermal energy storages. *Energy Procedia*, 91, 197–206.

Richter, M., Habermann, E.M., Siebecke, E., Linder, M. (2018). A systematic screening of salt hydrates as materials for a thermochemical heat transformer. *Thermochimica Acta*, 659, 136–150.

Ring, T.A., Dirksen, J.A., Duvall, K.N., Jongen, N. (2001). $LiBr \cdot 2H_2O$ crystallization inhibition in the presence of additives. *Journal of Colloid and Interface Science*, 239, 399–408.

Ristić, A. and Henninger, S.K. (eds) (2014). Sorption composite materials for solar thermal. In *Energy Procedia*. Elsevier, Amsterdam.

Rouquerol, J., Avnir, D., Fairbridge, C.W., Everett, D.H., Haynes, J.M., Pernicone, N., Ramsay, J.D.F., Sing, K.S.W., Unger, K.K. (1994). Recommendations for the characterization of porous solids (Technical Report). *Pure and Applied Chemistry*, 66(8), 1739–1758.

Rouquerol, F., Rouquerol, J., Sing, K. (1999). *Adsorption by Powder and Porous Solids: Principles, Methodology and Applications.* Academic Press, London.

Ruthven, D.M. (1984). *Principles of Adsorption and Adsorption Processes.* John Wiley & Sons, New York.

Sapienza, A., Glaznev, I.S., Santamaria, S., Freni, A., Aristov, Y.I. (2012). Adsorption chilling driven by low temperature heat: New adsorbent and cycle optimization. *Applied Thermal Engineering*, 32, 141–146.

Scapino, L., Zondag, H.A., Van Bael, J., Diriken, J., Rindt, C.C.M. (2017). Sorption heat storage for long-term low-temperature applications: A review on the advancements at material and prototype scale. *Applied Energy*, 190, 920–948.

Sharma, B. (2002). *Krishan's Objective Pre Engineering Chemistry*. Krishna Prakashan Media, Meerut.

Silva, V.M.T.M. and Rodrigues, A.E. (1999). Adsorption and diffusion in bidisperse pore structures. *Industrial & Engineering Chemistry Research*, 38(10), 4023–4031.

Simonova, I.A., Freni, A., Restuccia, G., Aristov, Y.I. (2009). Water sorption on composite "silica modified by calcium nitrate". *Microporous and Mesoporous Materials*, 122(1), 223–228.

Sircar, S. (2006). Gas sorption kinetics by differential closed-loop recycle method: Effect of heat of adsorption. *Adsorption*, 12(4), 259–266.

Sircar, S. and Myers, A.L. (2003). Gas separation by zeolites. In *Handbook of Zeolite Science and Technology*, Auerbach, S.M., Carrado, K.A., Dutta, P.K. (eds). CRC Press, Boca Raton.

Sögütoglu, L.C., Donkers, P.A.J., Fischer, H.R., Huinink, H.P., Adan, O.C.G. (2018). In-depth investigation of thermochemical performance in a heat battery: Cyclic analysis of K_2CO_3, $MgCl_2$ and Na_2S. *Applied Energy*, 215, 159–173.

Stadie, N.P. (2013). Synthesis and thermodynamic studies of physisorptive energy storage materials. PhD Thesis, California Institute of Technology, Pasadena [Online]. Available at: https://resolver.caltech.edu/CaltechTHESIS:09092012-010239493 [Accessed 8 December 2020].

Stitou, D. (2013). Transformation, conversion, stockage, transport de l'énergie thermique par procédés thermochimiques et thermo-hydrauliques. HDR, Université de Perpignan Via Domitia, Perpignan [Online]. Available at: https://tel.archives-ouvertes.fr/tel-00841655.

Stutz, B., Le Pierres, N., Kuznik, F., Johannes, K., Palomo Del Barrio, E., Bédécarrats, J.P., Gibout, S., Marty, P., Zalewski, L., Soto, J., et al. (2017). Storage of thermal solar energy. *Comptes Rendus Physique*, 18(7), 401–414.

Sugimoto, K., Dinnebier, R.E., Hanson, J.C. (2007). Structures of three dehydration products of bischofite from in situ synchrotron powder diffraction data ($MgCl_2 \cdot nH_2O$; n = 1, 2, 4). *Acta Crystallographica Section B Structural Science*, 63(2), 235–242.

Sun, L.M. and Meunier, F. (1987). Non-isothermal adsorption in a bidisperse adsorbent pellet. *Chemical Engineering Science*, 42(12), 2899–2907.

Sun, L.M., Meunier, F. (2003). Adsorption – Aspects théoriques. *Techniques de l'Ingénieur*, J2730, 1–16. doi: 10.51257/a-v1-j2730.

Sun, L.M., Meunier, F., Brodu, N., Manero, M.H. (2016). Adsorption – Aspects théoriques. *Techniques de l'Ingénieur* [Online]. Available at: www.techniques-ingenieur.fr/base-documentaire/procedes-chimie-bio-agro-th2/operations-unitaires-extractions-fluide-fluide-et-fluide-solide-42332210/adsorption-j2730/.

Tanashev, Y.Y., Krainov, A.V., Aristov, Y.I. (2013). Thermal conductivity of composite sorbents "salt in porous matrix" for heat storage and transformation. *Applied Thermal Engineering*, 61(2), 401–407.

Tatsidjodoung, P., Le Pierrès, N., Luo, L., Heintz, J., Lagre, D. (2014). Étude du fonctionnement d'un réacteur de zéolithe pour le stockage thermochimique de chaleur. In *Actes du Congrès de la Société Française de Thermique*. Société Française de Thermique, Lyon.

Teo, H.W.B., Chakraborty, A., Kayal, S. (2017). Post synthetic modification of MIL-101(Cr) for S-shaped isotherms and fast kinetics with water adsorption. *Applied Thermal Engineering*, 120, 453–462.

Thomas, W.J. and Crittenden, B. (1998). *Adsorption Technology and Design*. Elsevier, Amsterdam.

Tian, B., Jin, Z.Q., Wang, L.W., Wang, R.Z. (2012). Permeability and thermal conductivity of compact chemical and physical adsorbents with expanded natural graphite as host matrix. *International Journal of Heat and Mass Transfer*, 55(15/16), 4453–4459.

Tokarev, M., Gordeeva, L., Romannikov, V., Glaznev, I., Aristov, Y.I. (2002). New composite sorbent $CaCl_2$ in mesopores for sorption cooling/heating. *International Journal of Thermal Sciences*, 41(5), 470–474.

Tournoud, C. (2008). Les intoxications accidentelles domestiques par inhalation. In *Actes de URGENCES 2008, 2e Congrès de la Société Française de Médecine d'Urgence (SFMU)*, Paris [Online]. Available at: www.sfmu.org/upload/70_formation/02_eformation/02_congres/Urgences/urgences2008/donnees/pdf/045_tournoud.pdf [Accessed 5 May 2020].

Tso, C.Y. and Chao, C.Y.H. (2012). Activated carbon, silica-gel and calcium chloride composite adsorbents for energy efficient solar adsorption cooling and dehumidification systems. *International Journal of Refrigeration*, 35(6), 1626–1638.

Wagman, D.D., Evans, W.H., Parker, V.B., Schumm, R.H., Halow, I., Bailey, S.M., Churney, K.L., Nuttall, R.L. (1982). The NBS tables of chemical thermodynamic properties. Selected values for inorganic and C1 and C2 organic substances in SI units. *Journal of Physical and Chemical Reference Data*, 11, 2385.

Wang, X., Zimmermann, W., Ng, K.C., Chakraboty, A., Keller, J.U. (2004). Investigation on the isotherm of silica gel + water systems. TG and volumetric methods. *Journal of Thermal Analysis and Calorimetry*, 76, 659–669.

Wang, R., Wang, L., Wu, J. (eds) (2014). Mechanism and thermodynamic properties of physical adsorption. In *Adsorption Refrigeration Technology*. John Wiley & Sons, New York [Online]. Available at: onlinelibrary.wiley.com/doi/abs/10.1002/9781118197448.ch3.

Weber, R. and Dorer, V. (2008). Long-term heat storage with NaOH. *Vacuum*, 82, 708–716.

Weber, R., Asenbeck, S., Kerskes, H., Drück, H. (2016). SolSpaces – Testing and performance analysis of a segmented sorption store for solar thermal space heating. *Energy Procedia*, 91, 250–258.

Whiting, G., Grondin, D., Bennici, S., Auroux, A. (2013). Heats of water sorption studies on zeolite $MgSO_4$ composites as potential thermochemical heat storage materials. *Solar Energy Materials and Solar Cells*, 112, 112–119.

Wirth, E., Guitteny, F., Mathonat, C. (2014). Thermogravimétrie. *Techniques de l'Ingénieur*, 1–21 [Online]. Available at: www.techniques-ingenieur.fr/base-documentaire/mesures-analyses-th1/methodes-thermiques-d-analyse-42384210/thermogravimetrie-p1260/.

Wong, B., van Helden, W., Rosen, M.A. (2013). Compact thermal energy storage for potential Canadian market applications. In *3rd Climate Change Technology Conference, CCTC 2013*, Montreal [Online]. Available at: www.cctc2013.ca/Papers/CCTC2013%20TRA1-3%20Wong.pdf.

W. R. Grace & Co.-Conn. (2010). GRACE Davison/SYLOBEAD. Adsorbents for process applications [Online]. Available at: grace.com/general-industrial/en-us/Documents/sylobead_br_E_2010_f100222_web.pdf [Accessed 1 September 2020].

Wu, H., Wang, S., Zhu, D. (2007). Effects of impregnating variables on dynamic sorption characteristics and storage properties of composite sorbent for solar heat storage. *Solar Energy*, 81(7), 864–871.

Yu, N., Wang, R.Z., Lu, Z.S., Wang, L.W., Ishugah, T.F. (2014). Evaluation of a three-phase sorption cycle for thermal energy storage. *Energy*, 67, 468–478.

Zettl, B., Englmair, G., Steinmaurer, G. (2014). Development of a revolving drum reactor for open-sorption heat storage processes. *Applied Thermal Engineering*, 70(1), 42–49.

Zhang, Y.N., Wang, R.Z., Zhao, Y.J., Li, T.X., Riffat, S.B., Wajid, N.M. (2016). Development and thermochemical characterizations of vermiculite/ SrBr2 composite sorbents for low-temperature heat storage. *Energy*, 115, 120–128.

Zheng, X., Ge, T.S., Wang, R.Z. (2014). Recent progress on desiccant materials for solid desiccant cooling systems. *Energy*, 74, 280–294.

Zondag, H.A., van Essen, V.M., Bakker, M., Bach, P.W. (2010). An evaluation of the economical feasibility of seasonal sorption heat storage. In *Proceedings of the 5th International Renewable Energy Storage Conference (IRES 2010)* [Online]. Available at: www.ecn.nl/docs/library/report/2010/m10096.pdf.